Rizik od pojave rezonancije ili ferorezonancije u visokonaponskim mrežama istosmjernog napona

Radečić, Iva

Master's thesis / Diplomski rad

2024

Degree Grantor / Ustanova koja je dodijelila akademski / stručni stupanj: **University of Zagreb, Faculty of Electrical Engineering and Computing / Sveučilište u Zagrebu, Fakultet elektrotehnike i računarstva**

Permanent link / Trajna poveznica: https://urn.nsk.hr/urn:nbn:hr:168:202069

UNIVERSITY OF ZAGREB
FACULTY OF ELECTRICAL ENGINEERING AND COMPUTING

MASTER THESIS No. 101

RISK OF ELECTRIC RESONANCE OR FERRORESONANCE IN HVDC NETWORKS

Iva Radečić

Zagreb, September 2024

UNIVERSITY OF ZAGREB
FACULTY OF ELECTRICAL ENGINEERING AND COMPUTING

MASTER THESIS No. 101

RISK OF ELECTRIC RESONANCE OR FERRORESONANCE IN HVDC NETWORKS

Iva Radečić

Zagreb, September 2024

UNIVERSITY OF ZAGREB
FACULTY OF ELECTRICAL ENGINEERING AND COMPUTING

Zagreb, 04 March 2024

MASTER THESIS ASSIGNMENT No. 101

Student:	**Iva Radečić (9996006846)**
Study:	Electrical Engineering and Information Technology
Profile:	Electrical Power Engineering
Mentor:	assoc. prof. Božidar Filipović-Grčić
Co-mentor:	Bruno Jurišić, PhD

Title: **Risk of electric resonance or ferroresonance in HVDC networks**

Description:

The energy transition will very likely lead in the medium term to a significant development of HVDC transmission, in particular because of the large distances from electricity production centers to consumption centers, congestions in existing AC network, and the necessity to have better control of load flow and electricity transits. Converter operation results in both the generation of current harmonics art AC/DC side and the absorption of reactive power. In order to limit the negative impact of these currents harmonics the converter station normally includes shunt connected switchable AC harmonic filter and DC filters. HVDC links can contribute to saturation problems by bringing a DC offset in transformers or they may introduce harmonics that can lead to an increased magnetizing current in transformers, which, in turn, can contribute to saturation. Star-point reactors are usually used for this purpose. The presence of filters or inductance banks at the input or output of HVDC converters can lead to the existence of overvoltages linked to resonance or ferroresonance phenomena likely to damage the equipment. This issue is mentioned in various international documents, but there are few (or no) publications referring to real configurations. In this thesis, it is necessary to investigate and determine the configurations and operating conditions leading to resonance / ferroresonance, based on numerical simulations of electromagnetic transients carried out with the EMTP software. Possible mitigation solutions should be proposed and discussed to avoid the negative impact of phenomena on HV equipment.

Submission date: 06 September 2024

SVEUČILIŠTE U ZAGREBU
FAKULTET ELEKTROTEHNIKE I RAČUNARSTVA

Zagreb, 4. ožujka 2024.

DIPLOMSKI ZADATAK br. 101

Pristupnica:	**Iva Radečić (9996006846)**
Studij:	Elektrotehnika i informacijska tehnologija
Profil:	Elektroenergetika
Mentor:	izv. prof. dr. sc. Božidar Filipović-Grčić
Komentor:	dr. sc. Bruno Jurišić

Zadatak: **Rizik od pojave rezonancije ili ferorezonancije u visokonaponskim mrežama istosmjernog napona**

Opis zadatka:

Energetska tranzicija sa prijelazom na obnovljive izvore energije vrlo vjerojatno će dovesti do značajnog razvoja HVDC prijenosa u srednjem roku, posebno zbog velikih udaljenosti od centara proizvodnje električne energije do potrošačkih centara, zagušenja u postojećoj AC mreži te potrebom za boljom kontrolom tokova snaga i tranzita električne energije. Rad frekvencijskih pretvarača rezultira generiranjem strujnih harmonika na AC/DC strani pretvarača te apsorpcijom jalove snage. Kako bi se ograničio negativni utjecaj ove pojave, pretvaračka stanica uobičajeno uključuje filtre na AC i DC strani. U pretvaračkim HVDC stanicama može doći do problema sa zasićenjem energetskih transformatora uslijed pojave DC komponente struje te viših harmonika koji mogu uzrokovati povećanu struju magnetiziranja. Zbog toga se u HVDC stanicama obično ugrađuju prigušnice za uzemljenje u spoju zvijezda. Prisutnost filtera ili prigušnica na ulazu/izlazu iz HVDC pretvarača može dovesti do nastanka prenapona povezanih s rezonancijom ili ferorezonancijom, što može oštetiti visokonaponsku opremu. Ovaj problem spominje se u raznim međunarodnim publikacijama, ali postoje rijetke publikacije koje se odnose na stvarne konfiguracije mreže. U ovom radu potrebno je istražiti i odrediti konfiguracije mreže i pogonske uvjete koji dovode do pojave rezonancije/ferorezonancije, temeljem rezultata numeričkih simulacija elektromagnetskih prijelaznih pojava koje je potrebno provesti u EMTP softveru. Potrebno je predložiti potencijalna rješenja kojima se mogu ublažiti negativni utjecaji prethodno opisanih pojava na visokonaponsku opremu.

Rok za predaju rada: 6. rujna 2024.

This study was produced during a student internship as part of the collaboration between Electricité de France (EDF), France, and the Faculty of Electrical Engineering and Computing (FER), Croatia. The work has been done at EDF Lab in the Research and Development department.

First and foremost, I would like to thank Electricité de France for providing the opportunity for this internship. My gratitude also goes to my colleagues in the Research and Development department, especially to my tutors, Paul Akiki, PhD., and Alain Xémard, PhD., for their support and knowledge during the preparation of this work. I would also like to thank my mentor, Božidar Filipović Grčić, Assoc. Prof., and co-mentor, Bruno Jurišić, PhD., from the Faculty of Electrical Engineering and Computing. Their advice and suggestions have been invaluable at every step of this process.

I also extend my thanks to all the professors and colleagues at the Faculty of Electrical Engineering and Computing who have contributed to my education and personal development.

I am especially grateful to my family and friends for their unwavering support, understanding, and motivation throughout my studies. †

Table of Contents

List of Figures

List of Tables

Introduction

The use of power electronics in traditional high voltage alternating current (HVAC) systems is on the rise. Evidence of this lies in the adoption of new technologies such as flexible AC transmission systems (FACTS), converters for connecting smaller energy sources, usually renewable, and the use of high voltage direct current (HVDC) transmission. With the development of the free market, the need for increasingly frequent management of power flows arises. However, this is complicated by the limitations of the existing HVAC network, which does not provide the desired flexibility.

To prevent congestion caused by centralized production (areas rich in renewable energy sources) or centralized consumption (growing cities and industrial centres), the system is forced to introduce new technologies such as HVDC. HVDC technology, which brings with it well-known advantages, also introduces problems related to stability and the danger of possible oscillations. With the introduction of HVDC technologies, additional capacitances and inductances are introduced into the system which increases the risk of resonance and ferroresonance. Furthermore, the fact that the system itself is designed with very low resistance to reduce the need for cooling, also reduces the possibility that the resulting oscillations will dampen themselves over time [1].

There are some reports related to recorded oscillations, which are mostly associated with the phenomena of resonance near the HVDC system. Additionally, problems with intermediate torsional stresses between the turbine-generator and the HVDC station have also been recorded. Table 1 provides an overview of these issues.

As can be seen from Table 1, there are several recorded oscillations of various frequencies, ranging from just a few Hertz to several thousand Hertz. Based on it, the most logical division of oscillations is into subsynchronous oscillations (frequencies less than the nominal frequency of the network, 50/60 Hz) and supersynchronous oscillations (frequencies above the nominal frequency of the network, 50/60 Hz).

Table 1. Recorded cases of oscillations associated with HVDC stations [2]

Year	Location	Frequency [Hz]
2011	Nanhui, China	20-30
2013	BorWin1, Germany	451
2014	Nan'ao, China	20-30
2014-2017	OWF, Germany	1500
2015	Xiamen, China	23.6 – 25.2
2015	Inelfe, France-Spain	1700
2016	OWF, Germany	830
2016	Luxi, China	1270
2016	Zhoushan, China	> 1000
2018	YongFu, China	2.5 & 97.5
2018-2019	YuE, China	700 & 1800

Subsynchronous oscillations include electrical resonances, but also torsional ones. In the subsynchronous region, power electronic device interactions can also occur. On the other hand, supersynchronous oscillations are mostly electrical, but their division is not so straight as the subsynchronous. The topic of this paper is about electrical resonances, for which stability analysis is additionally complicated by their wide frequency range, which can be subsynchronous but also supersynchronous. Therefore, it is necessary to find an adequate, fast, and accurate method that will cover the entire frequency bandwidth for resonance stability issues.

Small-signal stability analysis, which includes modal analysis (i.e., eigenvalue) as well as frequency and time domain stability analysis, is one method which can be used for the analysis of oscillations [3]. The key to this method is to cause a disturbance after which it is checked whether the system will return to a stable point or whether it will cause further oscillations.

The aim of this paper is to provide an overview of the available methods for resonance analysis near HVDC networks. During the review of the available literature, a lack of studies that confirm analytical stability derivations with simulations in numerical programs such as

electromagnetic transient (EMT) programs has been revealed. Therefore, the goal is to provide an overview of real network configurations that are susceptible to electrical resonances. Additionally, an overview of ferroresonance, a special case of resonance, is investigated.

This document consists of several chapters. Chapter 1 serves as an introduction to the issue of HVDC and HVAC system interaction, while Chapters 2 and 3 present a more detailed description and classification of subsynchronous and supersynchronous oscillations in networks rich with power electronic devices. This leads to Chapter 4, which serves as an overview of the available methods for stability analysis. Chapter 5 attempts to link the available methods with temporary overvoltage studies and provides a review of the available literature. It also represents the main objective of this work.

Chapter 6 describes numerical approach for studying temporary overvoltages induced by electrical resonances. Next, Chapter 7 describes the process of obtaining the frequency response of the observed network in a numerical tool, i.e., an EMT program (EMTP). Time-domain simulations of recorded resonances are also addressed in Chapter 7. Chapter 8 is dedicated to the special case of ferroresonance, and finally, the Conclusion is presented. Additionally, used Abbreviations are provided at the very end of the document.

1. HVDC-HVAC Interaction Issues

Power electronic installations often lead to abnormal interactions and interoperability issues with AC networks. These phenomena can disrupt the stability and reliability of the power system, necessitating careful design and control strategies to mitigate their effects. The foundation for good analysis and the study of oscillations in networks dominated with power electronic devices is their classification.

The most common classification of oscillations in a power electronics dominated network is into subsynchronous and supersynchronous. The fundamental distinction lies in subsynchronous oscillations encompassing all phenomena oscillating at frequencies lower than the nominal frequency (less than 50/60 Hz), whereas supersynchronous oscillations include all other phenomena at higher frequencies (more than 50/60 Hz).

The oscillation division based on the new classification of subsynchronous resonances provided in CIGRE TB 909, with additional division of supersynchronous oscillations is illustrated in Figure 1 [3]. Chapters 2 and 3 describe more in detail a particular type of oscillation based on the division shown in Figure 1.

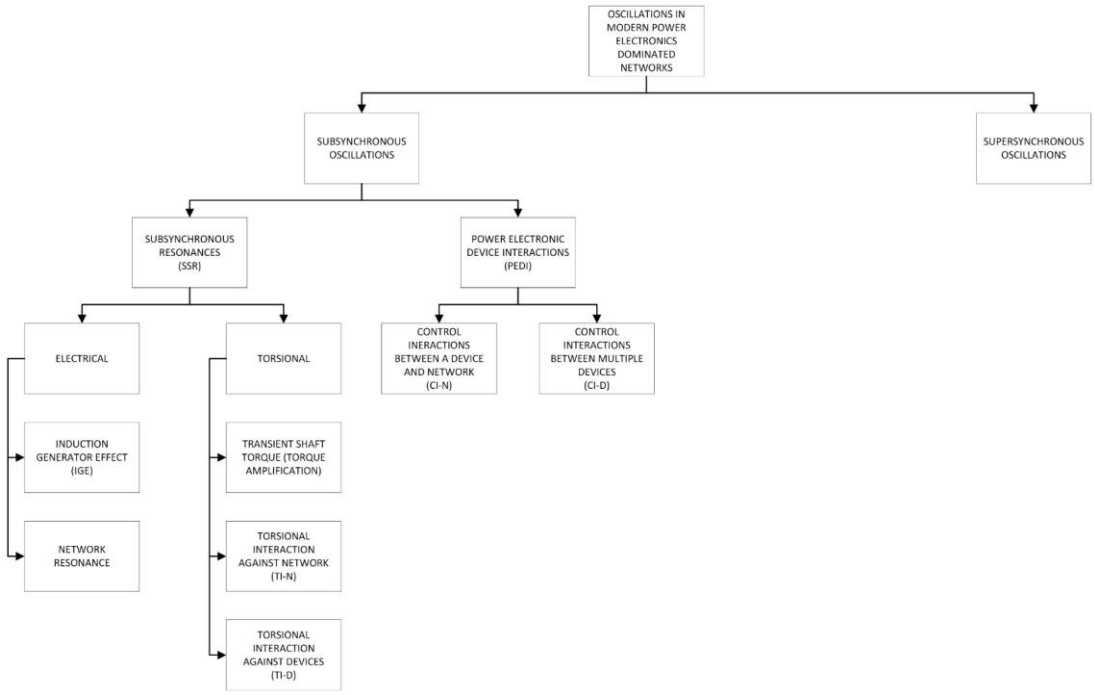

Figure 1. Division of oscillations in power electronics dominated networks

2. Subsynchronous Oscillations

As defined earlier, subsynchronous oscillations include all phenomena that oscillate with a frequency lower than the nominal frequency of the system (50/60 Hz). They include resonances, as well as the interaction of power electronic devices based on the division shown in Figure 1. The subsections of this chapter provide more detailed descriptions of them.

2.1. Subsynchronous Resonances

Subsynchronous resonances (SSR) can be purely electrical, but also torsional. Purely electrical resonances include the induction generator effect (IGE) and classic network resonance, while torsional resonances refer to transient shaft torques, torsional interaction against network (TI-N) as torsional interaction against devices (TI-D).

2.1.1. Electrical Resonances

The IGE occurs when an induction generator behaves like an inductance that resonates with the capacitive network, which is common in compensated transmission lines. Similar situations occur when wind turbines are connected via converters to the network that is series compensated. These resonances are purely electrical and arise as a result of the negative resistance of the rotating machine or converter [3].

A special case of network resonance is the subsynchronous controller interactions (SSCI) phenomenon, often referred to as Wind-SSCI, which does not involve mechanical interactions. Instead, it arises from the rapid and direct nature of the wind turbine rotor-side current controller loop. While controller parameters influence the phenomenon, controllers themselves do not actively participate. It should be classified as a form of subsynchronous resonance (SSR), originating from the destabilization of a network resonance mode by the converter controller.

2.1.2. Torsional Resonance

On the other hand, there are also torsional resonances, resulting from the matching of resonant frequencies between the mechanical shaft and the AC grid or converter. The proximity of a shaft resonance frequency (the subsynchronous complement) and a network resonance frequency results in large swings of shaft torque when a disturbance, such as a short circuit fault, occurs in the network. This phenomenon causes significant oscillations and is considered a large disturbance, resulting in transient shaft torques.

When it comes to torsional resonances, they are also possible against network or other power electronic device. TI-N resonance in the electrical network is caused by series capacitors that are commonly installed to compensate for the reactance of long transmission lines. The resonance as seen by a turbine generator in the network is translated to the rotor side at a subsynchronous frequency ($f_r = f_s - f_e$), where f_s is the synchronous frequency (e.g., 50 Hz), f_e is the frequency of electrical resonance (e.g., 30 Hz), and f_r is the resonant frequency translated to the rotor side (e.g., 20 Hz) [3]. If the net damping is negative, the torsional oscillation can grow and cause torsional fatigue damage to the shaft, which can result in cracks and other shaft component damage.

On the other hand, TI-D resonance causes torsional stresses in the shaft due to the interaction between the turbine and an electronic device, which can also include HVDC converters. These interactions occur in the subsynchronous region and can appear even in uncompensated networks. Their trigger does not have to be a network fault or a normal operation, but they can arise as a result of the operation of the converter control loops. An example of this phenomenon is the resonance between a wind farm connected via a converter (type 4) and the grid, whose frequency matched the torsional frequency of a nearby turbine in a thermal power plant [3]. The phenomenon itself was not triggered by anything specific but lasted for 3 hours and 20 minutes, leading to the emergency tripping of the thermal power plant.

2.2. Power Electronic Device Interactions

Experiences reported in the literature include two types of power electronic device interactions (PEDI). In the first type, a power electronic device interacts with the network. In the second type, two power electronic devices interact with each other across the network. Usually, the controllers of these devices are responsible for the interactions, and therefore, it is commonly referred to as subsynchronous controller interaction [3].

2.2.1. Between a Device and Network

Control interactions between a device and the electrical network are defined as CI-N. The difference between CI-N and the IGE is that, in IGE, the negative damping is introduced by the electrical system of a synchronous generator, which behaves as an induction generator in the subsynchronous frequency range.

In [3], a case of TI-N interaction between a wind farm and the grid is described, where the authors refer to the phenomenon as "DFIG control participated induction generator effect," which is purely electrical without the involvement of torsional dynamics.

2.2.2. Between Multiple Devices

CI-D involves interactions between power electronic devices (converter and controls) and another electronic device, in contrast to CI-N which focuses on interactions between a device and the electrical network.

2.3. Quick Survey

In the previous subsections of Chapter 2, a review of the subdivision of subsynchronous oscillations in a network with a predominant number of power electronic devices is provided. A quick survey of the described interactions is presented in Table 2.

Table 2. Quick survey of subsynchronous oscillations [3]

<table>
<tr><th colspan="2">Main category</th><th>Subcategory</th><th>Interacting component A</th><th>Interacting component B</th></tr>
<tr><td rowspan="6">Subsynchronous resonance (SSR)</td><td rowspan="3">electrical</td><td>IGE</td><td rowspan="3">series capacitors
L-C resonant circuits (filters, line shunt compensation)</td><td>synchronous and asynchronous machines (generators, motors)
WTG type 1-3</td></tr>
<tr><td>network resonance</td><td>power electronics (converter and controls)</td></tr>
<tr><td>wind-SSCI</td><td>WTG type 3</td></tr>
<tr><td rowspan="3">torsional</td><td>transient shaft torques</td><td rowspan="3">synchronous machines (generators, motors)
WTG type 1-3 shaft</td><td>series capacitors (transient)</td></tr>
<tr><td>TI-N</td><td>series capacitors
(steady state)</td></tr>
<tr><td>TI-D</td><td>power electronics (converter and controls)</td></tr>
<tr><td colspan="2" rowspan="2">Power electronic device interaction (PEID)</td><td>CI-N</td><td rowspan="2">Power electronics (converter and controls)
WTG type 3-4, inverter based resources, converters (HVDC, FACTS, SVC)</td><td>AC (weak) grid</td></tr>
<tr><td>CI-D</td><td>Power electronics (converter and controls)</td></tr>
</table>

3. Supersynchronous Oscillations

Of particular interest are the supersynchronous oscillations associated with the increasing number of power electronic devices in the grid. These oscillations are still insufficiently understood. Currently, there is no relevant CIGRE document that provides a methodological classification of these oscillations, as is the case with subsynchronous oscillations described in [3].

The main issue is that the development of HVDC technology was initially based on line commutated converters (LCC), whose overall influence was significantly based on converter transformer and large filters. However, with the advancement of voltage source converters (VSC), which not only generates significantly less harmonics but also includes configurations where filters are not required, the situation has changed. The fundamental difference between LCC and VSC lies in the type of switch they are based on. LCC is based on a semi-controlled switch such as a thyristor, whereas VSC is based on a fully controlled switch such as an IGBT or similar. It is therefore likely that with the increased use of VSCs, whose high-frequency control system has a larger impact than that of LCCs, there is a shift from subsynchronous oscillations to supersynchronous ones, which are also referred to as "harmonic oscillations" in [4].

When it comes to harmonics, two situations need to be considered: 1) the converter itself acts as a source of harmonics, and 2) certain harmonics are already present in the network [4]. To study the harmonic generation by a converter, it is essential to understand its operation. VSC produces an output voltage as a stepped function, which ultimately results in integer harmonics and can also lead to the creation of interharmonics [4]. The situation is further complicated with the introduction of modular multilevel converter (MMC), a special type of VSC based on more controllable voltage, whose harmonic production differs significantly from the classical VSC converters with two or three-level control. The difference in their spectrum is illustrated in Figure 2.

The increased peaks for the harmonic order higher than 500 can be seen, which is a characteristic of the MMC. However, this response is merely indicative and primarily depends on valve control. However, a sudden increase in amplitudes in the high-frequency range can significantly affect system stability and pose a risk of potential oscillations. Furthermore, the presence of existing harmonics on the AC side and their impact on stability

must not be overlooked as converter can amplify its magnitude. All in all, harmonics are not desirable in the network because, in addition to distorting the existing current and voltage waveforms, they also increase the risk of triggering possible resonances.

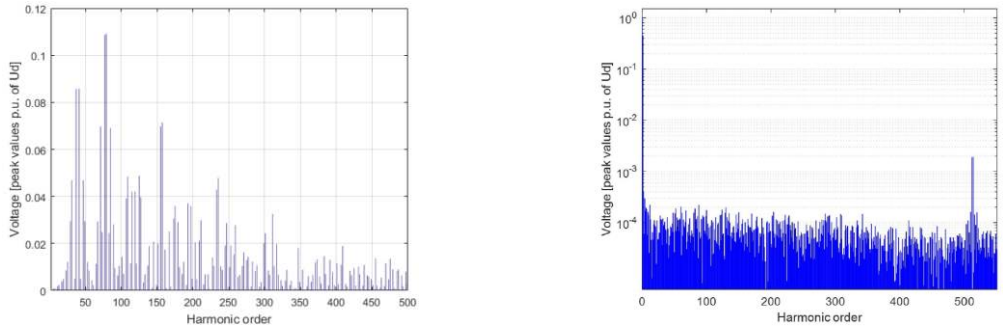

a) harmonic spectre of three-level VSC

b) harmonic spectre of MMC

Figure 2. Difference between harmonic spectrum of three-level VSC and MMC [4]

The key to consider the issue of harmonic stability lies in understanding the concept of harmonic impedance, i.e., the frequency response of the impedance of individual parts of the network. The problem arises when the converter can no longer be viewed as strictly passive impedance (due to the significant influence of tuned filters), and its active side, i.e., the control system, must also be considered.

Generic representation of the interaction between the passive part of the converter (Z_T and Z_R as characteristics of the converter transformer and reactor) and the active (C_V and C_I as transfer functions of voltage and current control loops) is shown in Figure 3. Chapter 4 describes the available methods for stability analysis, which include obtaining the frequency response of both converter impedances together.

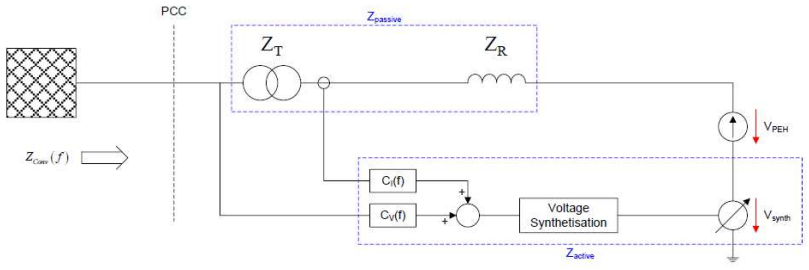

Figure 3. Interaction between active and passive elements of converter [4]

The harmonic stability is primarily associated with VSC devices, whose total impedance is heavily influenced by the active part (i.e., control), as opposed to LCC, where the total impedance is masked by the passive impedance of the filter. The control system operates at higher frequencies than nominal, hence this problem can be considered supersynchronous.

4. Stability Analysis

As previously mentioned, a key aspect of analysing the stability of a system with a high penetration of converter-based devices is to encompass a wide frequency range. In the context of converter-based power systems, small-signal stability refers to the system's ability to return to a limited steady-state after a minor disturbance. This encompasses the dynamic behaviour of converters across multiple time scales, where disturbances can occur either below (subsynchronous) or above (supersynchronous) the fundamental frequency of the power system. The small-signal dynamics of converters can introduce negative damping across various frequency ranges, influenced by both the controller type and the power system conditions. Based on this, three fundamental methods have been developed to apply this approach:

1. eigenvalue-based stability analysis,
2. stability analysis in frequency domain,
3. stability analysis in time-domain simulation [5].

Earlier mentioned oscillations related to network stability have mostly been observed from the AC side. However, they also need to be considered from the DC side. Oscillation frequencies on the AC side can vary widely, but it has been shown that lower frequencies are mostly influenced by converter outer control, while higher frequencies are more related to inner control. However, oscillations and instability can also be observed from the DC side, which also encompasses a wide frequency range.

From the above, it can be concluded that understanding the operation of converters, and thus their control loops, is of utmost importance in stability analysis. The absence of data from the converter side creates an issue that necessitates the converter to be presented as a black box. The control of the MMC, the most promising type of VSC, are cascaded according to their bandwidth [5]. The cascade control system of the MMC converter is depicted in Figure 4.

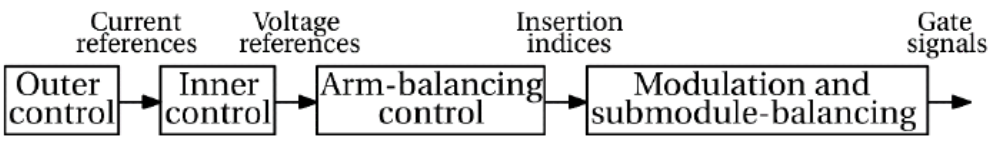

Figure 4. MMC cascaded control system [5]

The slowest component is the outer control, which can include direct voltage control (DVC), active power control (APC), reactive power control (RPC), alternating voltage control (AVC), and droop control. The phase-locked loop (PLL), which is crucial for synchronizing the converter with the grid, is also considered part of the outer control [5]. Outer control loops operate in the frequency range of up to several hundred Hertz, and their operation provides a reference for the faster inner control [6].

Inner control loops are much faster and operate in the frequency range from around a hundred Hertz up to kilohertz. They include an output current control (OCC) and a circulating current control (CCC). Additionally, converter topologies with distributed energy storage like MMC, also require control algorithms for capacitor voltage balancing (CBA). When it comes to their implementation, it is typically done using PI controllers. After the outer and inner control loops, there are significantly faster arm-balancing control, modulation, and submodule-balancing control.

The described cascade approach to the operation of control loops in MMC converters is key to later gaining a better understanding of their impact on network stability analysis. The previously mentioned methods for stability analysis are described in more detail in the following subchapters. Understanding the operation of control loops will play an important role in better comprehending each specific analysis.

Once the cascaded approach to converter control and its operation in general is understood, the stability analysis can be started, with the main methods being based on both analytical and numerical approaches, as explained further in the subchapters. Thus, the eigenvalue method, as well as methods that can be conducted in both the frequency and time domains, are described.

4.1. Eigenvalue-based Stability Analysis

Stability analysis based on modal analysis (i.e., eigenvalue analysis) views the system as a combination of several independent oscillatory and non-oscillatory modes. In the context of power systems, this method has predominantly been used to investigate low-frequency oscillations and subsynchronous oscillations [5].

It is important to note that for this method, the system must first be linearized around the operating point, which is most often determined by the converter's loading level. Linearizing

a nonlinear model inherently introduces certain deviations from the real system, and the overall linearization process can sometimes be challenging.

The next step in conducting modal analysis is determining the Jacobian matrix around the previously defined operating point, after which its eigenvalues (i.e., the poles of the system), are calculated. The Jacobian matrix is a matrix of all first-order partial derivatives of a vector-valued function, representing the linear approximation of the system dynamics around that specific operating point.

Based on the obtained eigenvalues, it is possible to determine the stability of the system. Broadly speaking, the system is classified as stable if all calculated eigenvalues in the Jacobian matrix have a negative real part [5]. Additional analysis of individual eigenvalues can provide a more detailed insight into stability. The classification of each mode can be further described by calculating the attenuation, frequency, and relative damping of each eigenvalue.

If the stability condition is not satisfied or is critical, it is possible to explore which part of the individual system contributes most to the impending instability using participation factor analysis [5]. Based on that, it can serve as a useful tool in system operation optimization and prevention of undesired oscillations.

The main limitation of this method is its linearization, meaning that the analysis is valid only around the previously defined operating point. It is also important to note that modal analysis is predominantly performed in the dq system. Therefore, it is necessary to transform the existing three-phase system into the dq system using Park's transformation. This can be problematic when dealing with MMC converters, whose variables contain not just a single frequency component (0 Hz (DC) or 50/60 Hz (AC)), but at least two or more frequencies simultaneously, even under balanced conditions. Additionally, this method requires comprehensive knowledge of all converter controls, which manufacturers are not obligated to provide as it is part of their intellectual property (IP), further complicating the process.

4.2. Stability Analysis in Frequency-domain

The study of stability, unlike modal analysis, can also be performed in the frequency domain. There are two main methods for this: the transfer function-based method and the impedance-based method. The transfer function method relies on the closed-loop transfer functions of the system. This approach allows the implementation of network-side impedance into the system, which can also affect the control system of the converter.

On the other hand, the impedance-based method views the system as two distinct parts, the AC side and the DC side, and examines their interaction at the point of common coupling (PCC) using the Nyquist stability criterion. A significant advancement in the impedance-based model is that the converter can now be treated as a black box. This greatly simplifies the analysis, as the manufacturer only needs to provide the frequency response of the converter without the need for additional knowledge of the system's control loops, which is necessary in the transfer function method and the previously described modal analysis.

4.2.1. Based on Transfer Function

One possible method for verifying the stability of a grid-connected converter is through the representation of the system, its various control levels, and variables using transfer functions. These transfer functions can then be easily displayed in the frequency domain, after which well-known theories of linear controls can be applied. However, this process is not straightforward as it involves the use of complex space vectors as well as complex transfer functions, most commonly utilizing the Laplace transform. The process becomes further complicated if the system is considered asymmetrical, which is often the case in reality.

The procedure itself, which can be quite complex as described, utilizes the generalized Nyquist stability criterion and the multivariable Bode criterion.

4.2.2. Based on Impedance

The stability check based on impedance was first introduced by Middlebrook in 1970 during the design of DC/DC converters, where the system was divided into load and source subsystems, with the ratio of source output impedance to load input impedance required to satisfy the Nyquist stability criterion [5]. This method was later generalized and is now applied to HVDC systems. Its significant advantage lies in the protection of IP, thereby addressing one of the issues of previously mentioned methods. Additionally, it is less time

consuming than getting the frequency response from time domain simulations using some EMT program.

The procedure is reduced to an equivalent electrical circuit depicted in Figure 5, where the system block diagram is also illustrated. In contrast to Middlebrook's approach, which involved a source and a load, the AC side is now represented as a voltage source, while the DC side is represented as a current source. The current between these subsystems can be further described by equation (1). Based on (1) the minor-loop gain $L(s)$ can be written as (2). The system described in this manner can be considered stable if the minor-loop gain is stable, which is demonstrated using the Nyquist criterion. However, initially, it is necessary to establish that $L(s)$ has no poles in the right-half plane. This method should not be confused with the earlier transfer function-based approach, as transfer functions are also utilized in this procedure. However, unlike the previous method, in this approach, the AC and DC sides are considered separately.

a) equivalent circuit b) block diagram

Figure 5. Representation of interconnected AC and DC system [5]

$$I(s) = \frac{I_l(s)Z_l(s)}{Z_s(s) + Z_l(s)} - \frac{U_s(s)}{Z_s(s) + Z_l(s)} = \left(I_l(s) - \frac{U_s(s)}{Z_l(s)}\right) \cdot \frac{1}{1 + Z_s(s)/Z_l(s)} \quad (1)$$

$$L(s) = \frac{Z_s(s)}{Z_l(s)} \quad (2)$$

The idea of this method is not to simplify the transfer function method, but to treat the AC and DC systems as two separate systems. This way, the frequency response of the AC side and the frequency response of the DC side impedances are observed independently and then applying the Nyquist criterion as further described.

H. Saad, et al., in [7], have described an analytical derivation for obtaining the MMC converter impedance $Z_{MMC}(s)$. When deriving an analytical expression, they excluded consideration of the upper-level control loops while investigating resonance within the frequency range of 100 to 3000 Hz. Additionally, circulating current and balancing control were disregarded, with focus solely on the AC side. This simplification is based on the fact

of different frequency bands of operation of individual controls in the converter, which are described at the beginning of the Chapter 4. Network topology and obtained transfer function for the generic MMC station is shown in Figure 6.

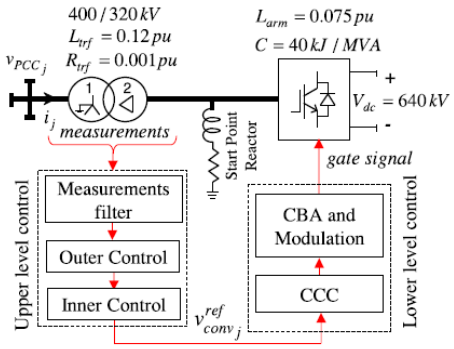

a) Network topology and control system

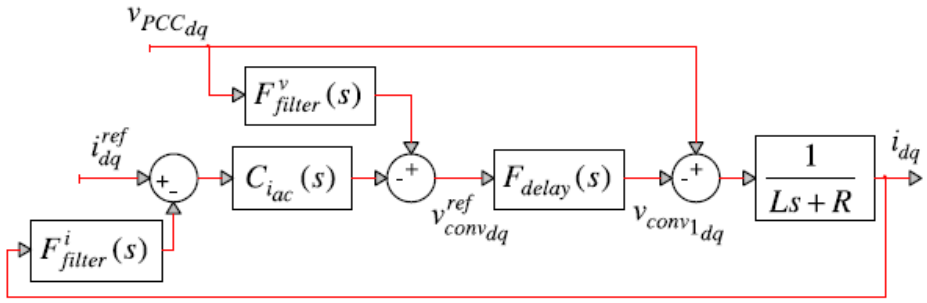

b) Transfer function

Figure 6. Generic structure of MMC station [7]

Following Figure 6, the equation of the impedance of the converter (3) can be set, where other transfer functions are also part of it. The equation includes $C_{i_{ac}}$ as the PI control loop, ${F_{filter}}^{v}$ as the low pass filter of the feedforward voltage $v_{PCC_{dq}}$and ${F_{filter}}^{i}$ as the low pass filter of the measured current. F_{delay} is the transfer function that helps in linearizing the dead time of the converter. The dead time of a converter is a brief delay between switching transistors to prevent a short circuit. It ensures safe operation by avoiding simultaneous conduction of both switches.

$$\frac{v_{PCC_{dq}}}{i_{dq}} = Z_{MMC}(s) = \frac{Ls + R + C_{i_{ac}}(s){F_{filter}}^{i}(s)F_{delay}(s)}{1 - F_{delay}(s){F_{filter}}^{v}} \tag{3}$$

By a similar procedure, the AC side impedance can also be obtained, allowing for the application of the generalized Nyquist stability criterion. The stability margin is typically

determined graphically using a Bode plot, as the Nyquist plot lacks direct frequency value (Figure 7). To ascertain system stability, the phase response is analysed at every frequency point where the converter and the network impedance intersect in their magnitude responses. Each intersection signifies a series resonance between the converter and the grid, with the phase disparity indicating the degree of net damping at that resonance frequency. Specifically, the resonance is positively damped if the phase difference $\Delta\varphi$ is less than 180°, undamped if $\Delta\varphi = 180°$, and negatively damped (unstable) if $\Delta\varphi > 180°$ [8]. The key is that the larger the phase angle exceeds 180 degrees, the greater the amplification will be, which directly leads to instability.

In Figure 7, the frequency response of the AC impedance and the DC converter is depicted, with the phase difference observed at each intersection of their impedance magnitudes. It can be noted that at a frequency of 1025 Hz, the impedance magnitudes intersect with a phase difference exceeding 180°, indicating unstable resonance.

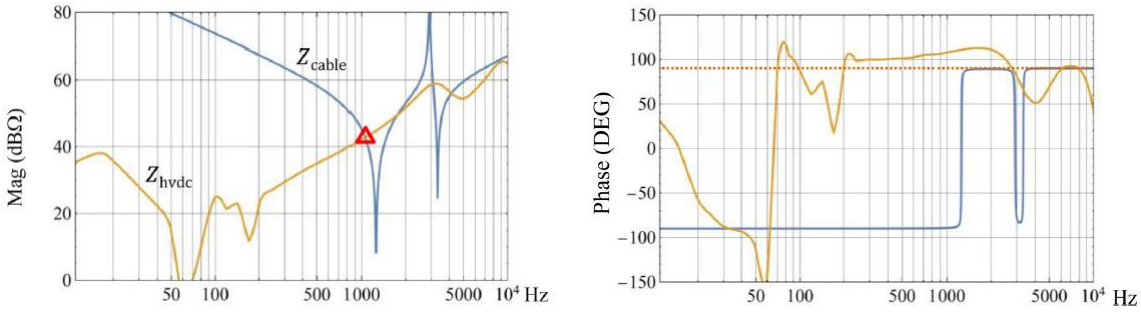

Figure 7. Example of frequency response of the AC (blue) and DC (yellow) side impedance [8]

In the impedance-based method, an analytical technique is employed to determine the equivalent impedance as a function of frequency from the perspective of the device under analysis for which stability is being analysed. It aids in identifying the most likely real-world scenarios in the network that could lead to resonance. However, this method serves merely as indicative, as a more detailed analysis must necessarily involve EMT time-domain analysis [5]. It is also important to note that when modelling individual system components, it is necessary to consider their frequency-dependent models to consider the wide frequency band of the possible occurrence of resonance [3].

Building upon this method, the passivity-based approach emerged, asserting that oscillations can be prevented if the converter exhibits passive behaviour across the entire frequency spectrum (the phase angle of the impedances is between 90° and –90°). With such an approach, it would be ensured that if the converter behaves as purely inductive (90°) and the

network as purely capacitive (–90°), the total phase shift would be 180°, which would place the system at the very edge of stability, but not in the unstable region. However, when it comes to the converter, it is difficult to achieve its passivity, especially at higher frequencies [4]. Forcing the passivity of the converter brings additional costs, raising further questions about its feasibility. It is crucial to emphasize that while passivity positively influences the stability, it does not solely determine it. Thus, stability can still be achieved even if the converter behaves non-passively.

According to assertions in [9], primary sources of instability stem from the constant power control of the converter (manifesting as negative resistance despite positive input) and the dynamics of the control loop. Overall, impedance-based methods for stability analysis solve the problem of not knowing the control structure and easily assess stability across a wide frequency range, and their implementation is relatively fast compared to other observed methods.

4.3. Stability Analysis in Time-domain Simulation

Stability analysis of the system can also be performed through time-domain simulation. In the field of power systems, there are two main types of software programs that are used: the electromagnetic transients (EMT) programs and root-mean-square (RMS) programs.

The primary difference between them lies in the time step used for simulation. RMS simulations are based on much larger time intervals, enabling their applications to large-scale systems, albeit with a limited frequency range. In contrast, EMT programs can cover a broader frequency spectrum [5]. Therefore, it can be stated from the outset that EMT programs are more suitable for studying stability and oscillations over a wide frequency range.

Analysing stability, which is conducted in frequency domain, can be achieved by injecting a small perturbation at each frequency during time domain simulation using small signal perturbation in EMT programs [10]. The key is to compute the necessary variables for every injected frequency, which, in the event of stability will be impedance. Equivalent harmonic circuit of the EMT model is shown in Figure 8. Usually current injection is used, while voltage injection is less common in practice. Also, Figure 8 displays a graphical representation of how to transform from the time domain to the frequency domain.

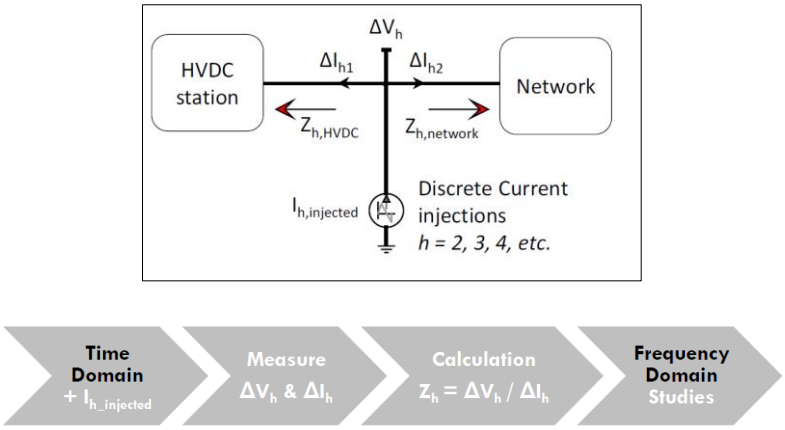

Figure 8. Transition from time to frequency domain in EMT program [4]

The use of EMT programs in stability analysis brings several advantages. Firstly, they enable the verification of linearized models based on black-box models. As previously mentioned, the analytical process involves linearization, which is further complicated by the fact that the accuracy of the created model remains uncertain due to the IP constraints imposed by the converter manufacturers. The use of EMT models allows for a detailed description of individual converter functions. For instance, the impedance-based model proposed by H. Saad et al. was verified using the EMTP program, as the EMT converter model provides a more detailed description of controls compared to analytical model. The results are shown in Figure 9, where a slight deviation can be observed in the low-frequency range (< 400 Hz). This deviation is attributed to the previously mentioned neglect of the outer control loops, as higher frequency band is analysed (100 – 3000 Hz).

Although the practice so far has been to validate EMT models by comparing them with analytical models, which in most cases have served as benchmarks, it appears that due to the increasing complexity of systems (especially converters, which control is unknown), there is an inevitable need for the reverse situation, in which analytical expressions are verified using EMT models which are based on generic control loops.

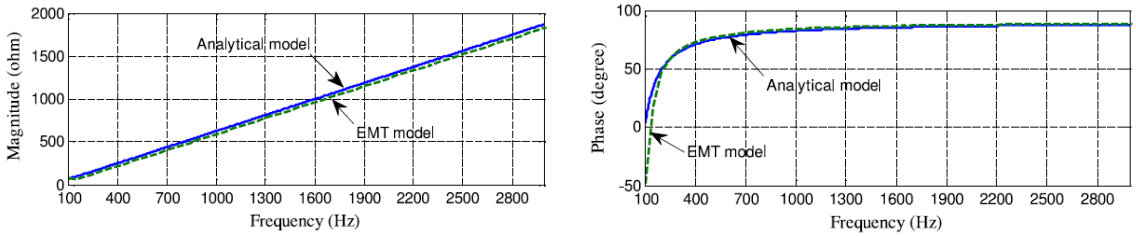

Figure 9. Difference between analytical and EMT response of $Z_{MMC}(s)$ [7]

Additionally, EMT modelling facilitates the inclusion of harmonics near HVDC stations, which are known sources of harmonics. In the paper mentioned earlier [7], an effort was made to include harmonics analytically using a basic current source. Harmonics, generated by the converter's operation, alter the current and voltage waveforms, and can induce resonance, making them crucial in resonance analysis. EMT programs incorporate harmonics by providing a thorough depiction of the converter's operation at switching level, making their results more reliable compared to those that overlook harmonics which is a common occurrence in analytical calculations.

Figure 10 compares the harmonic emissions of MMC analytically and through EMT simulation. Although MMC typically has very low harmonic emissions, differences are visible, especially at lower frequencies (< 400 Hz). Nevertheless, some high-frequency harmonics present in the analytical analysis (1250, 1550, and 2450 Hz) are not observed in the EMT simulation. This discrepancy arises from the analytical difficulty in modelling the winding of the transformer, particularly when it is a delta configuration, which eliminates induced harmonics in the EMT simulation. Neglecting transformer windings, along with control loops, can reduce the reliability of analytical results.

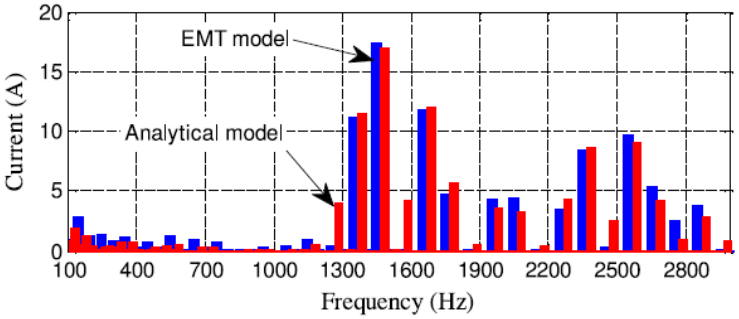

Figure 10. Difference between analytical and EMT harmonic emission of MMC [7]

Another, and primary, advantage is that it enables the implementation of non-linear control loops as well as other non-linear components, such as transformer saturation. EMT programs enable this in a much simpler way compared to the highly demanding and complex nature of analytical calculations, which always involve some simplification methods, consequently leading to less accurate results. This advantage enables the study of phenomena such as ferroresonance in converter transformers.

It is also confirmed in [7] and [11] that time delay primarily affects the phase angle of the impedance response at frequency, while its impact on the magnitude is negligible. The time delay refers to the time shift between the reference signal and the actual operation of the

converter to ensure smooth and precise control, as its value increases, the phase angle of the converter also increases, as shown in Figure 11.

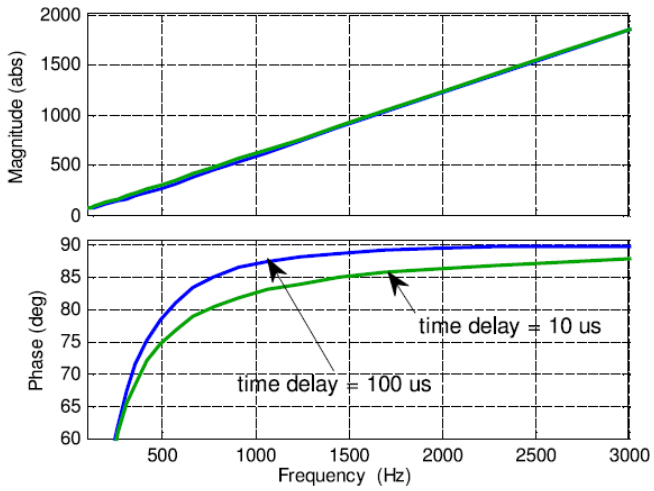

Figure 11. Impact of time delay on the frequency response of the converter [7]

From all the above, it can be concluded that the converter control system plays an important role in the study of resonant phenomena. A key role in this is played by the time constants of the control loops, whose influence on *Z(s)* is studied in articles [7] and [11]. Inner control, which includes the current control and capacitor balancing, has a higher influence on high frequency response of the converter, while they respond in that frequency range. The higher the time constant of the inner control, the converter behaves as an inductor, while a lower time constant leads to capacitive behaviour of the converter which is confirmed in [7].

Although numerical programs such as EMTP offer numerous advantages in defining the details of individual component designs and network topology, they also come with long simulation times, which can sometimes be extended, primarily due to the need for a small time step in simulations to maintain accuracy.

However, attention must be paid when using all the capabilities of EMT models. Specifically, care must be taken when defining individual components that need to be represented as frequency-dependent to ensure accurate results [3]. This modelling approach provides wide frequency applicability, allowing for the analysis of both subsynchronous and supersynchronous oscillations.

5. Temporary Overvoltage Studies

Sudden network changes, faults, interruptions, or improper equipment handling can lead to the occurrence of overvoltages. An overvoltage is any voltage between a phase conductor and ground or between two phase conductors, whose peak value exceeds the corresponding peak value of the highest permissible operating voltage [12]. It is an undesirable consequence of an electrical power system because it imposes additional stress on insulation, unwanted heating, which ultimately results in accelerated insulation aging, equipment damage, additional losses, and in extreme cases, system failure.

For a better understanding of overvoltages, the standard IEC 60071-1 is used, which categorizes overvoltages into three main categories:

1. temporary overvoltages,
2. transient overvoltages,
3. combined overvoltages [12].

Temporary overvoltage (TOV) is an overvoltage of relatively long duration, which can be undamped or weakly damped. In some cases, its frequency can be several times lower or higher than the operating frequency. Phenomena such as resonance, ferroresonance, the Ferranti effect, etc., lead to temporary overvoltages. On the other hand, transient overvoltages are short duration overvoltages lasting several milliseconds or shorter, oscillatory or non-oscillatory, usually heavily damped. Additionally, they are divided into slow front, fast front, and very fast front transient overvoltages. Events such as switching operations, lightning strikes, etc., are associated with these types of overvoltages [13].

The primary focus of this study is electrical resonance and ferroresonance, which lead to transient overvoltages in accordance with IEC standards. Their primary concern is not voltage amplitude, as equipment is designed to tolerate higher levels. Instead, the focus is on their extended duration, leading to excessive heat generation, raising the risk of thermal damage and explosion hazards for personnel. Additionally, ferroresonance is characterized by insulation aging and magnetostriction-induced noise. Distorted waveforms with harmonics and subharmonics degrade power quality and might prompt unnecessary activation of protection systems [13].

HVAC and HVDC interactions also include the concept of electrical resonance which is related to the equality of the inductive and capacitive part of the network of a particular area. The analytical analysis of electrical resonance is usually based on the study of the frequency response of the AC and DC side impedance at PCC (i.e., impedance based method) [10].

The issue arises from the fact that, despite discussing the impedance of HVDC converters, it is not solely determined by the physical characteristics of the HVDC network, such as resistance, inductance, and capacitance values. Rather, it is influenced by a multitude of control loops implemented within the converter, including parameters such as firing angle and time delays [10].

As mentioned, analytical derivations of converter behaviour can be extremely demanding. Due to all the difficulties related to the complexity of the analytical analysis, as well as the implementation issues of certain parts of the network (e.g., converter controls and transformer winding), there is a growing need for other methods. The mathematics of converters and overall grid has become so complex that it is difficult to solve analytically, therefore, numerical methods implemented in simulation programs represent a promising solution. However, it is important to note that one cannot replace the other, and it is necessary to first validate models. For better understanding, Figure 12 illustrates the primary methods in analysing the risk of resonances within the network.

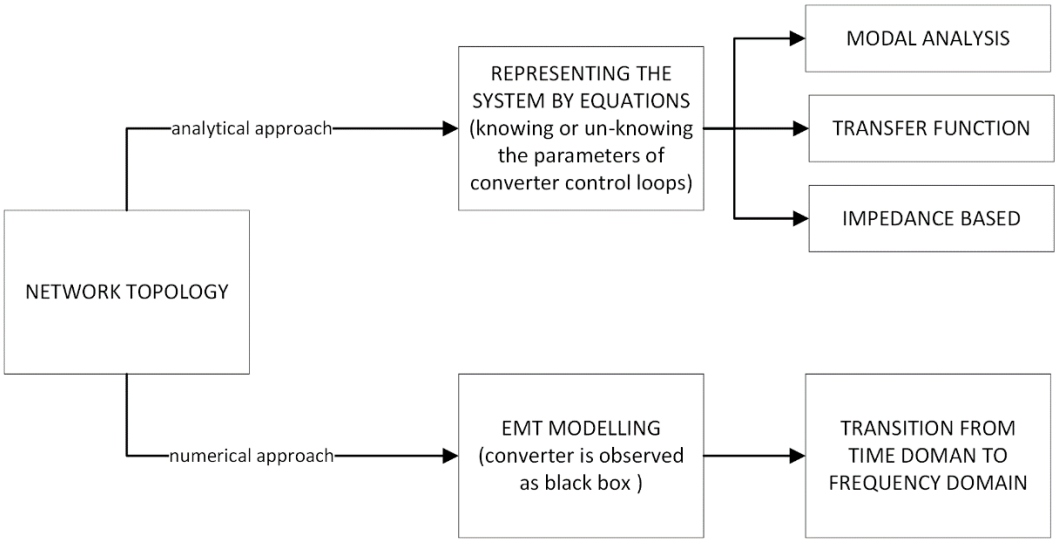

Figure 12. Available methods for stability analysis

The overall goal of overvoltage protection is to capture the worst-case scenario and investigate it to dimension equipment accordingly or limit the overvoltages using various methods. It can be said that studying stability based on electrical resonance and the

previously described methods is of utmost importance when examining TOVs. To capture the worst-case TOV on either the AC side or the DC side, the simulation should be conducted under specific system conditions as recommended below:

- set the system to the maximum system Short Circuit Level (SCL) and the lowest frequency at steady state, or alternatively, to the minimum system SCL and the highest frequency at steady state (these combinations can capture the worst-case resonant condition of the network),
- ensure the maximum steady-state AC voltage at the PCC,
- take into account the maximum transferred active power,
- consider the maximum consumed (inductive) reactive power [14].

In [14], it is also mentioned that TOV can be caused by events on the AC side of the interface transformer, within the valve side of the interface transformer, or due to a fault on the DC side. A special case is also related to the occurrence of ferroresonance on the converter transformer. Further subchapters provide some typical case studies related to the investigation of HVDC electrical resonances based on EMT programs.

5.1. Disconnection of Wind Turbines

In reference [10], a preliminary study was conducted for the FAB link project between the UK and France, which involves the connection of a 600 MW offshore wind farm to the DC link. The wind farm is connected via VSC converter. The aim is to investigate the possibility of resonance using EMT tools. Black-box converter models were used, as well as type 4 wind turbines. The network configuration is illustrated in Figure 13 and consists of six feeders, each with a capacity of 100 MW, connected to a busbar transformer. The cable length is assumed to be 5 km for each feeder.

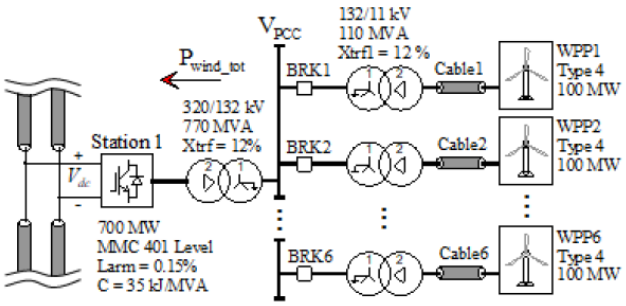

Figure 13. Network topology - offshore wind power station [10]

The study consists of both time-domain and frequency-domain simulations, focusing on the case of gradually disconnecting feeders every 0.5 seconds (one by one). The time response of power and voltage at the PCC is shown in Figure 14. After disconnecting the first and second feeders, the voltage manages to remain stable. However, at t=3.5 s, high-frequency voltage oscillations occur. The enlarged view of the observed resonance is shown in Figure 15, with an oscillation frequency of 830 Hz. Following this, a frequency analysis of the observed oscillation was conducted.

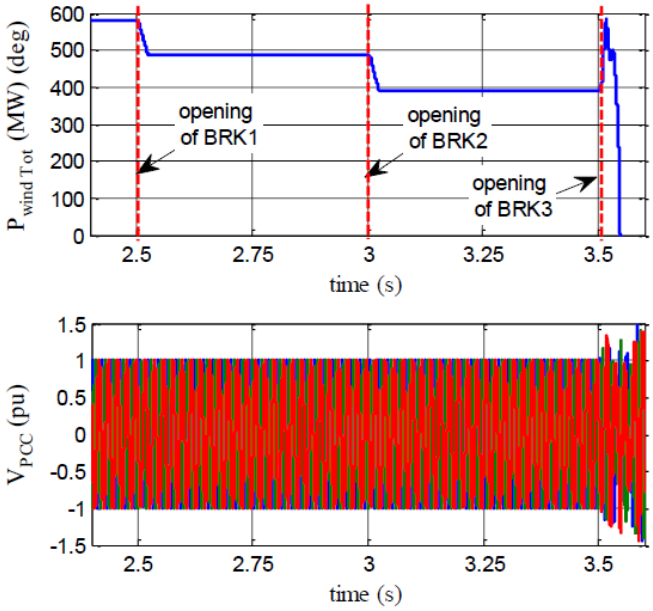

Figure 14. Time domain simulation of disconnecting WPP feeders [10]

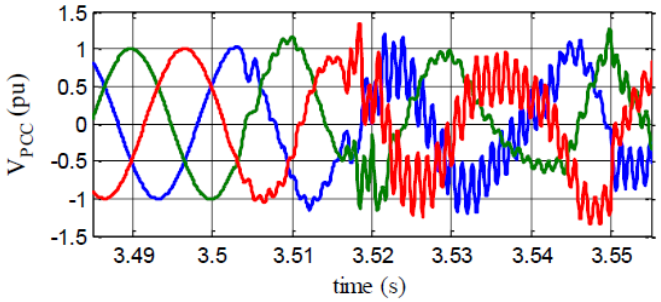

Figure 15. Zoomed waveform of voltage, oscillation with 830 Hz occurs [10]

The analytical investigation of this phenomenon is based on the frequency analysis of the impedance response of each side of the PCC. Thus, frequency responses of the impedance of the HVDC network and the Wind Power Plant (WPP) were obtained using the EMT tool.

Figure 16 illustrates the obtained results, emphasizing the change in frequency response as the available wind power varies. When the WPP operates at 500 MW, only one intersection

of impedances is observed at a frequency around 800 Hz. The phase difference is very close to 180°, so instability was not confirmed, but it is evident that it is compromised.

Conditions for instability are triggered by opening BRK3, altering the frequency characteristic of the WPP but not the HVDC network. Now, there are two intersections of curves at frequencies of 520 and 833 Hz. However, now the phase margin is greater than 180°, ultimately confirming the occurrence of the observed oscillation. Additionally, a negative damping of the wind power plant is observed at the intersection frequencies, while this is not observed in the HVDC grid. Based on this, it can be concluded that the cause of this instability is primarily the control of the WPP, rather than the control of the HVDC converter.

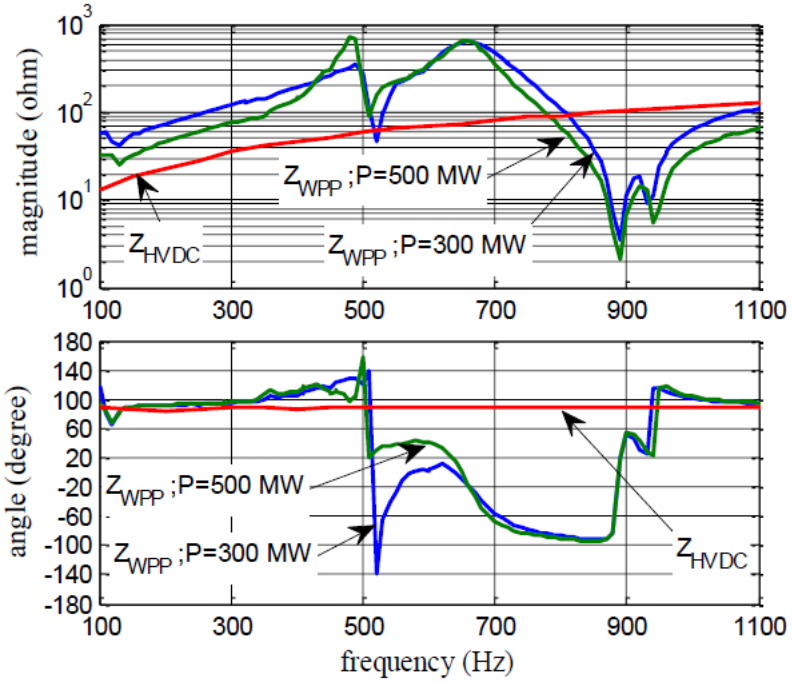

Figure 16. Frequency domain simulation of disconnecting WPP feeders [10]

5.2. Changing the Topology of the AC Network

When it comes to typical configurations of HVDC networks aiming to connect two HVAC networks, the state of the AC network and its changes can often cause resonance. Therefore, modelling the frequency response of the AC network is quite challenging, with the additional complication of its variability [15]. According to [15], due to the difference in impedances between the AC and DC sides, high-frequency resonance (defined as above 50 Hz in the

study) occurs. The impedance of the AC network changes along with its topology, hence it has multiple resonant points, which pose a danger during interaction with the DC system.

A special danger has been observed with long transmission lines, especially cables with high capacitance per unit length, which can lower the resonance frequency. Cable resonances near 250/300 Hz are particularly hazardous as these harmonics are often present on the AC side [1]. This can lead to system destabilization and potentially serious issues in the operation of the power system. Therefore, it is crucial to manage these factors carefully and take appropriate measures to prevent or minimize the negative consequences of resonance.

The work presented in the article [7] is based on the analysis of changes in the configuration of the AC network and the measurement of voltage at the PCC. The network configuration is illustrated in Figure 17. The given configuration is such that it transmits 1000 MW from Grid 1 to Grid 2 via two parallel AC overhead lines, and then through an MMC station. Additionally, the parallel lines are shunt-compensated with a power of 400 MVAr. The study examines how opening the BRK at t=0.5 s will affect the voltage at the PCC.

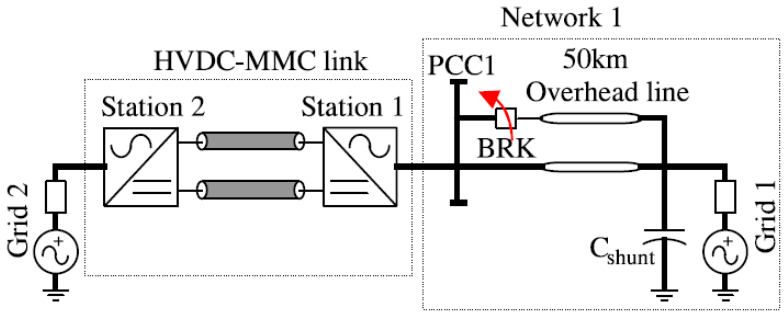

Figure 17. Network topology – changing the AC system topology [7]

The simulation was performed using EMTP software, the influence of the converter's low-pass filter, specifically its cutoff frequency, was also studied (F_{ci}=2 kHz; F_{ci}=200 kHz). The frequency response of AC grid and converter station is represented in Figure 18. It can be concluded that the frequency response of the AC network has changed after opening the BRK, it is also visible that the value of the cutoff frequency of the filter has minor influence on the magnitude of the impedance of the converter, but primarily affects its angle.

The phase difference becomes greater than 180° only when one of the AC lines is turned off at a frequency of about 1.7 kHz, which creates conditions for resonance. However, it can be observed that a higher cutoff frequency (200 kHz) reduces the total phase difference and thus helps to mitigate resonance effects, which is proven by the voltage time responses shown in Figure 19. Similar phenomena were recorded when the time delay was increased

[7]. This work is proof that even in networks with a large SCL, resonance is possible, although it is mostly always related to the concept of weak networks.

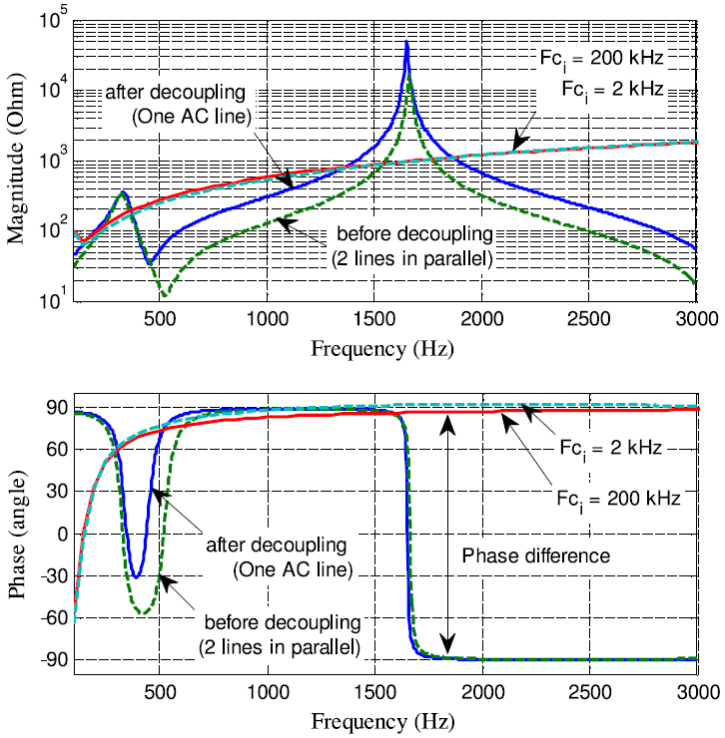

Figure 18. Frequency domain simulation - changing AC network topology [7]

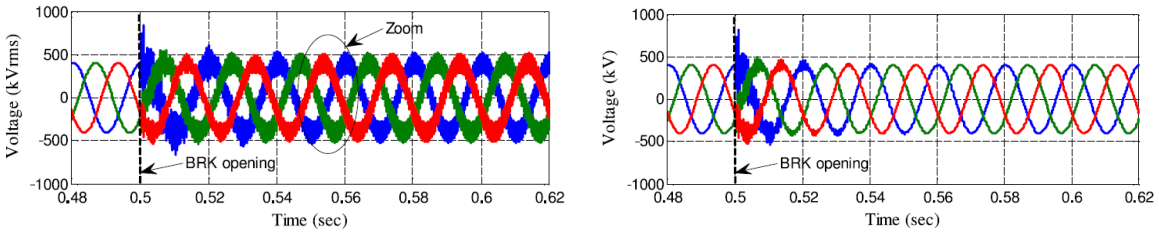

a) F_{ci}=2 kHz

b) F_{ci}=200 kHz

Figure 19. The influence of cutoff frequency on voltage waveform [7]

Disconnection of certain parts of the network can also occur as a result of faults, so in paper [16] an EMT simulation of a three-phase fault lasting 200 ms was made. The topology of the observed network, as well as the observed oscillations of voltages after removing the fault, are shown in Figure 20.

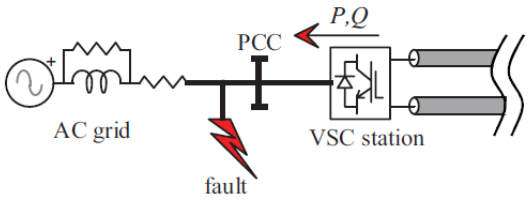

a) network topology

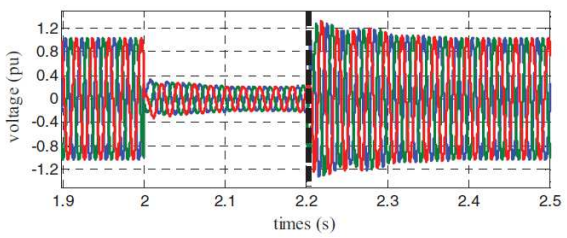

b) AC voltage at PCC

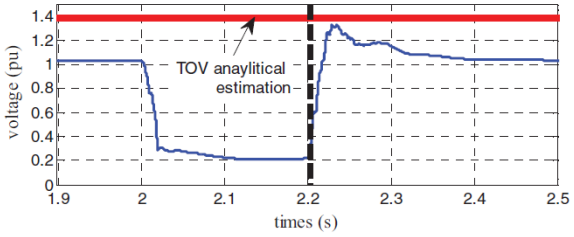

c) DC voltage at PCC

Figure 20. Transient overvoltages after fault recovery event [16]

An equation (4) is also presented that allows for a rough estimate of the maximum value of TOV in the network. This equation is derived from the method known in fast decoupled load flow, based on it, it is possible to calculate the voltage variation ΔV at the PCC:

$$\Delta V = -\frac{\Delta Q}{V}\frac{1}{B} \tag{4}$$

where ΔQ is the deviation of the reactive power and B is the total susceptance of the AC network at PCC [16]. An important parameter in the calculation of the maximum TOV is the deviation in reactive power, whose response change due to failure, as well as the response of the working power (shown in Figure 21).

As evident from the attached responses, the reactive power before the fault is -300 MVAr, while the active power is 1000 MW. During the fault, the control system provides reactive power support, stabilizing the reactive power at +200 MVAr. However, after the fault is cleared, the reactive power sharply increases to +860 MVAr. The cause of this increase is the control system, which requires time to react to the change in voltage. Based on this, it can be stated that the primary cause of the TOV is the difference in reactive power before and after the fault. Additionally, several other parameters can influence its magnitude, such as the operating voltage of the network, SCL, and active power.

This paper demonstrates that equation (4) can be used for a rough estimation of the maximum value of TOV. In the described case, using equation (4), a value of 1.39 p.u. was obtained, which is slightly higher than the peak value obtained from the EMT simulation, which is 1.33 p.u. (Figure 20.c).

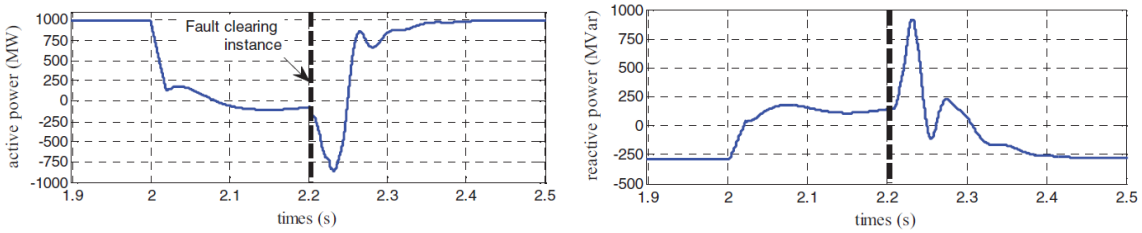

a) active power at PCC b) reactive power at PCC

Figure 21. Active and reactive power during and after the fault at PCC [16]

5.3. Two PE Devices Connected in Close Vicinity

It is a well-known fact that with the increasing penetration of power electronics (PE) into the existing grid, both its stability and overall inertia are compromised. In addition to reducing inertia, penetration of power electronics can cause problems with harmonic distortion, resonance, and TOV increases. These effects can further disrupt network stability and require careful analysis and management.

In article [16], an analysis of the maximum TOV values was conducted when two power electronics devices are connected to the busbar. The operation of the VSC converter was observed in three scenarios, with an LCC/SVC/VSC device connected to the same busbar, which topologies are shown in Figure 22.

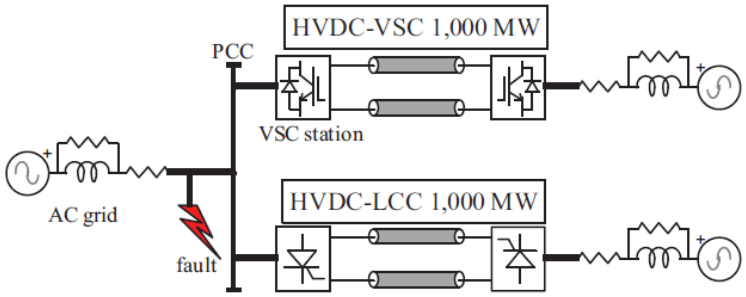

a) VSC - LCC busbar

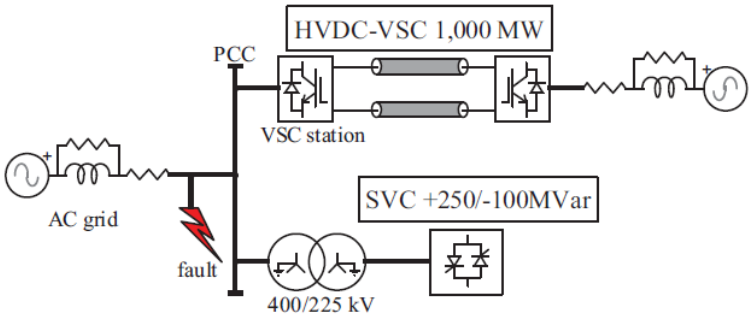

b) VSC – SVC busbar

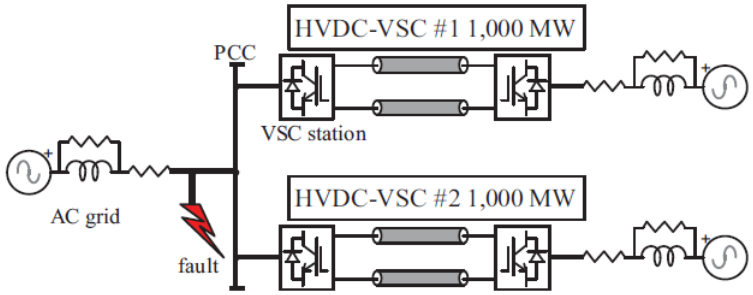

c) VSC – VSC busbar

Figure 22. Two PE at the same busbar network topologies [16]

A series of simulations were conducted using EMTP, with some simulations including the second PE device being turned on and then off, some parameters are also changed (P/Q setpoints, fault resistance, time of the VSC inner control).

Interestingly, in all three cases, it was observed that the amplitude of TOV increased when an additional PE device was connected alongside the existing VSC, and its duration was also prolonged. Figure 23 shows the maximum recorded TOV values in a total of 200 simulations in the case of two VSCs operating at the same busbar. The maximum TOV value increased from the previous 1.34 p.u. to 1.41 p.u. with the inclusion of an additional VSC converter on the busbar.

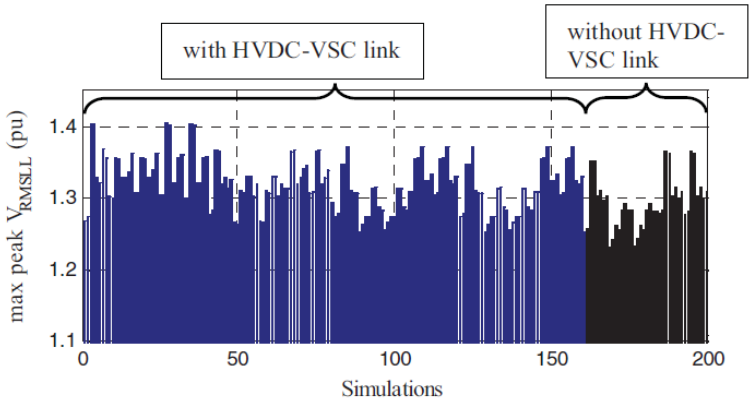

Figure 23. Maximum TOV value - two VSCs at the same busbar [16]

These results show that when PE devices are connected in close vicinity to a VSC link, higher TOV peak and longer TOV duration are to be expected. This is mainly due to three aspects: reduction of the short-circuit ratio of the system, the increase in reactive power support during the fault period, and control interaction between the HVDC-VSC link and the other PE devices [16].

6. Numerical Approach for Studying TOV

In a traditional power system stability analysis, the electromagnetic properties of the circuit are typically disregarded, as all active controls and dynamics primarily operate at low frequencies. However, VSC employ dynamics and control loops spanning a wide frequency spectrum, extending to significantly higher frequencies compared to conventional systems like synchronous machines or LCC. A VSC behaves as an active element, with its dynamics interacting with the electromagnetic characteristics of the network, potentially being influenced by resonances [4]. This interaction gives rise to a novel stability concern in power systems, often referred to as "harmonic stability" (which is in this study classified into supersynchronous oscillations, although its classification is still unclear).

Based on everything mentioned, it can be concluded that there are certain analytical and numerical methods for this analysis, with impedance-based method standing out due to its ease and simplicity of application. However, there remains the issue of modelling converters for higher frequencies, i.e., determining their impedance frequency response despite the IP problem and the complexity of the process itself. But the traditional AC side should not be neglected either, while its modelling becomes more uncertain with higher frequencies, as secondary effects (such as stray capacitance, skin effect and Eddy-current losses) become influential and so the analysis of the system to be investigated becomes progressively more complex. Therefore, it is necessary to pay equal attention to both AC and DC components, although DC components certainly represent a greater innovation in their implementation and operation.

As stated earlier, returning to Figure 3, the total impedance of the converter can be divided into an active and a passive component, where the active part is more pronounced with VSC than with LCC due to the previously mentioned reduced need for filters. Based on Figure 3, it is possible to derive an analytical expression for the impedance of the converter according to equation (5).

$$Z_{conv}(f) = \frac{C_I(f) + Z_T(f) + Z_R(f)}{1 - C_V(f)} \tag{5}$$

However, the question still arises how to model voltage and current controls if the relevant data from the manufacturer are not available. Furthermore, this wideband modelling is

further unclarified in standards, which typically recommend studying up to the 50th harmonic, which is insufficient with the introduction of power electronics [4].

There are some attempts to solve the aforementioned problems, one example being the implementation of generic converter control, which could rewrite equation (5) as equation (6), where G_{cc} and F_{ff} are current and filter controllers, while e^{-ts} represents the dead zone of the converter, i.e., time delay [4]. It is evident that equation (6) is closely related to the previously shown diagram in Figure 6 and equation (3), with very small deviations observed between the EMT model and the analytical approach.

$$Z_{conv}(f) = \frac{e^{-ts}G_{cc} + Z_T(f) + Z_R(f)}{1 - e^{-ts}F_{ff}} \tag{6}$$

However, such simplified approaches, as well as the use of generic models, still need to be approached with caution because each converter control is unique depending on its implementation. Nonetheless, if that is the only option available, it can still be very useful in addressing stability issues.

The main reason for implementing such generic loops lies in the fact that when studying this type of stability, the active impedance of the converter must be taken into account even if there is no information about its detailed model. This is evident from Figure 24, which shows the difference between the frequency response of a converter observed as passive and as active. There is a certain part of the impedance (above 1000 Hz) that poses a stability issue based on passivity criterion, and thus it cannot be overlooked. This especially applies to VSC converters, whose impedance is even more influenced by controls.

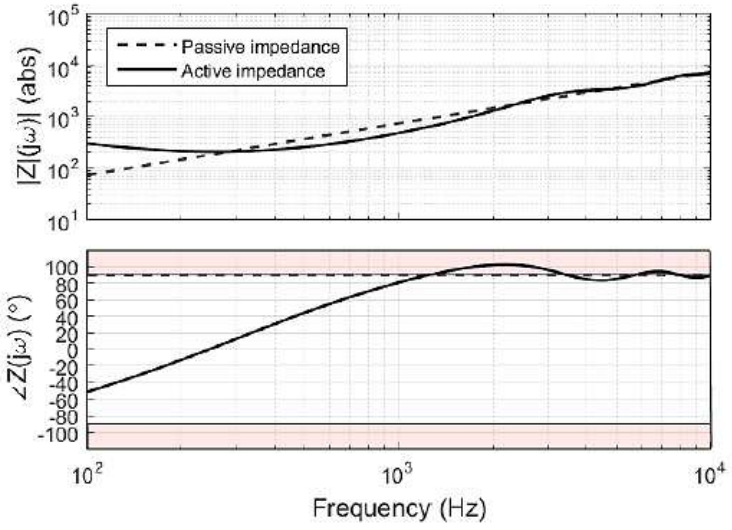

Figure 24. Difference between active and passive impedance of the converter [4]

The frequency response represented in Figure 24 reveals two distinct behaviours across the frequency spectrum. Between 100 Hz and 1000 Hz, the phase angle of the active impedance exhibits increasing damping compared to the purely inductive behaviour of the passive impedance. This increase in damping is attributed to the influence of the current control loop, which aims to regulate the current passing through the reactor with a constant proportional characteristic. Consequently, within this frequency range, the converter's response has a beneficial effect, damping the electromagnetic natural frequencies and alleviating network resonances if they exist.

Above 1 kHz, the behaviour significantly deviates. The phase angle of the impedance extends beyond the passive boundaries ($-90° < \varphi < +90°$) for certain frequency ranges, highlighted in red. These intervals correspond to an equivalent negative resistive behaviour, or active conductance, exhibited by the converter. As a result, the system damping decreases within these frequency ranges, making this area highly susceptible to the occurrence of TOVs in the network.

Addressing the issue of TOVs in complex electrical networks requires a precise understanding of dynamic interactions among various system components. While traditional analytical approaches are fundamental, they often entail complex calculations and result interpretation. Therefore, there is a growing inclination towards numerical methods, particularly utilizing EMT tools like EMTP, which offer faster and simpler simulations with high accuracy.

In the subsequent sections, numerical simulations based on EMTP will be presented, utilizing generic MMC converter models. Efforts have been made to adhere to the guidelines outlined in IEC standards as well as relevant documents such as CIGRE brochures. General guidelines for modelling and simulation in EMT programs can be found in standards like IEC 60071-4 and IEC 60071-11 [17]. When it comes to modelling VSC, TB 832 and TB 604 issued by CIGRE can be useful [18]. TB 604 is particularly important as it describes the first CIGRE benchmark for studying HVDC network.

EMT simulations should be sufficiently long, typically spanning a few seconds, to capture the effects of dynamic devices comprehensively. The HVDC model needs to incorporate accurate representations of key control functionalities, including DC voltage and power control, reactive power control, dynamic reactive current injection, and current limits. Additionally, protective functions that could trigger a converter trip or blockage due to

undervoltage or overvoltage should be accounted for. If a detailed EMT model is accessible, it is advisable to benchmark the simplified transient stability model against it.

There are four MMC models of varying complexity available in EMTP, their complexity is presented in Figure 25, while its description is briefly presented in Table 3. The choice of model to be used primarily depends on the available time and the analysis being conducted.

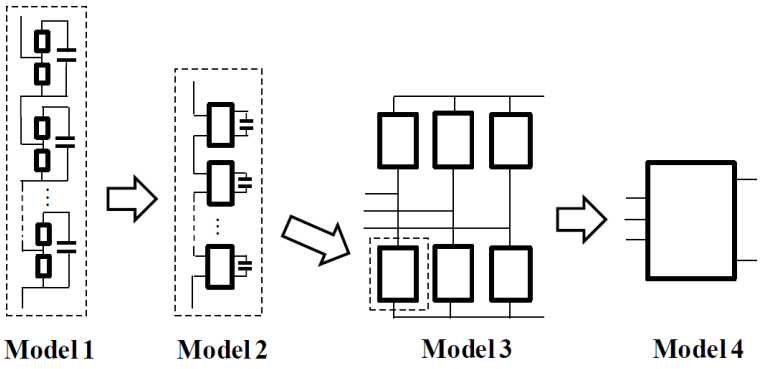

Figure 25. Available EMTP models based on complexity [19]

Table 3. Available MMC models in EMTP [19], [5]

EMTP MMC models	
Model 1 FULL DETAILED	- nonlinear IGBT and diode representation - every conduction mode of the MMC - highest computational time
Model 2 DETAILED EQUIVALENT	- switches are replaced by ON/OFF resistors in each submodule - eliminating nodes based on Norton equivalent for each MMC arm
Model 3 SWITCHING FUNCTION OF ARM	- equal capacitor voltage per cell - submodules are condensed into one equivalent units
Model 4 AVERAGE VALUE MODEL	- MMC is presented as controlled voltage and current sources - capacitors are perfectly balanced

The key is to validate any simplified model against measurements from an operational HVDC project. Alternatively, if obtaining such measurements is impractical, validation can

be conducted against a comprehensive model, usually in the time domain, which includes relevant parts of the control system (i.e., the simplified model can be validated by more complex model). A comparison of current responses for different converter models following a DC fault is illustrated in Figure 26. As evident, Models 1, 2, and 3 exhibit close alignment, whereas Model 4 diverges significantly. According to [4], Model 3 or Model 2 are suitable for EMT simulations to conduct harmonic and resonance studies, this information is important as further numerical simulations are based on Model 3.

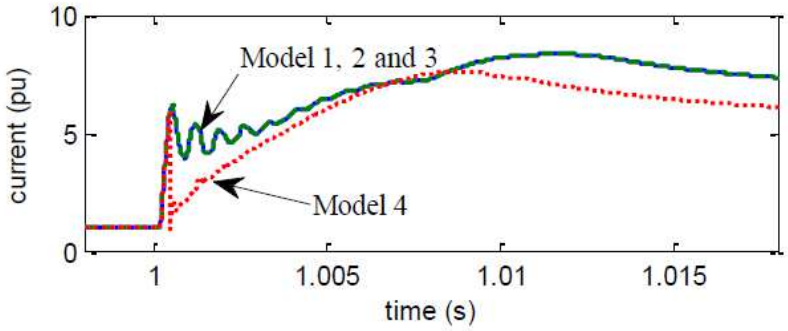

Figure 26. Difference between current response based on different MMC models [19]

Once a validated converter model is available and all components are presented as frequency-dependent, which is essential for TOVs analysis, the study of the configured network with all given parameters can be initiated. Observed network topology in this study is further described in the following Chapter 7.

7. Electrical Resonance

Before studying TOV caused by resonances, a network was created in the numerical program EMTP. Its topology is shown in Figure 27. Two networks represented by Thevenin equivalents are connected, Equivalent network 1 and 2, each with a Short Circuit Capacity (SCC) of 10 GVA and a nominal voltage level of 400 kV RMS LL. These networks are connected by a long AC cable and two MMC stations connected to DC cable, through which 1 GW of nominal power can be transmitted from Equivalent network 1 to Equivalent network 2 and vice versa. It is important to note that in all further presented cases transmitted power is 1 p.u., and the impact of changing this operating point was not part of this study.

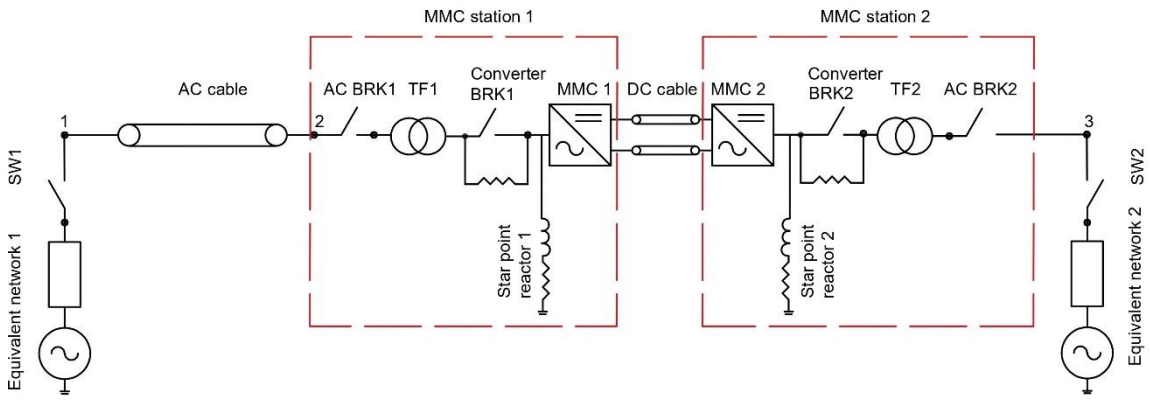

Figure 27. Case study - network topology

The unipolar 400 kV AC cable is placed in the ground at a depth of around 1 m, its length is 160 km. The cross-section of the AC cable is shown in Figure 28. This length was chosen to highlight the significant capacitance of the cables with an assumption that the resonance can be induced between the inductance of the converter and the capacitance of the cable. The properties of the cable were entered into the numerical program using a wideband cable model. Resistivity of the cooper core and sheath is $1.724 \cdot 10^{-8}$ Ωm, while the permittivity of the XLPE insulation is 3. Additionally, due to the cable length, it was necessary to implement compensation to reduce the current of parasitic capacitances to the ground. Thus, shunt compensation of 500 mH in every phase is added at each side of the cable. The AC cable connects Equivalent network 1 and the MMC station 1.

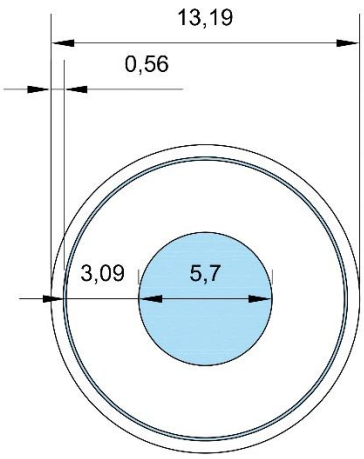

Figure 28. Cross-section of the AC cable (blue-conductor, in cm)

MMC stations are implemented using a generic model available in EMTP where the converter is represented as a black box. Each MMC station is described with its main components, AC breaker, converter transformer, converter breaker, star point reactor, and the converter, as is depicted in Figure 27. The converter transformer 400/320 kV RMS LL provides an AC voltage of 320 kV RMS LL for converter which is then used for the DC part of the network with a voltage level of ±320 kV DC. Two MMC stations are in monopole configuration and are connected with a 70 km DC cable, which is also implemented in the numerical simulation using wideband cable model. It is important to note that the magnetization branch of the converter transformers is only included in the MMC station 1, while in MMC station 2 it is excluded. This is done to achieve faster network stabilization as described further in the text. The converter transformers are in a star configuration on the AC side and in a delta configuration on the DC side, which is a common setup for these transformers. Main parameters of the used MMC station are presented in Table 4, while more details about its structure can be found in [19].

Overall, all parameters related to the DC components (MMC stations and DC cable) are based on the actual design for the planned 400 kV interconnection between the France and Spain networks as reported in [19].

Additionally, unless otherwise specified, all simulations were conducted using converter Model 3, previously described in Chapter 6. In this model, each MMC arm is averaged using the switching function concept of a half-bridge converter. Additionally, all simulations were conducted with a time step of 50 μs, and the converter operates from a steady state without the need for a start-up sequence with an initialization time of 0.2 s, as described in [19].

Table 4. MMC black box parameters

MMC parameters	
Type of model	Model 3 – switching function of arm
Configuration	Monopolar
Rated power	1000 MVA
AC primary/secondary voltage	400/320 kV RMS LL
Frequency	50 Hz
DC pole-to-pole voltage	640 kV
Transformer reactance	0.18 p.u.
Transformer resistance	0.001 p.u.
Transformer magnetization curve (Converter transformer 1 – TF1)	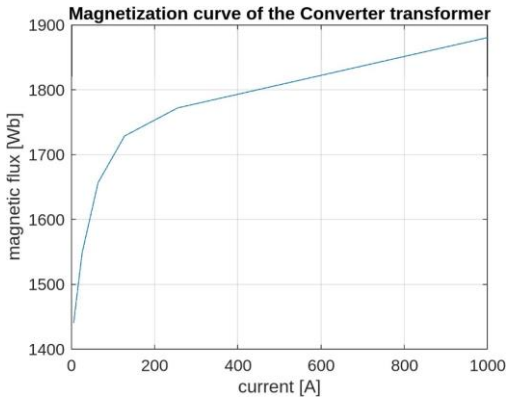
MMC arm inductance	0.15 p.u.
Capacitor energy in each Submodule	40 kJ/MVA
Number of submodules per arm	400
Conduction losses of each IGBT/diode	0.001 Ω
Star point reactor parameters	7700 Ω 6500 H
Inner current control time constant	0.01 s
DC current maximum limit protection	6 p.u.

Once the network topology has been designed and implemented in EMTP, it is necessary to analyse its steady state. As previously mentioned, in the steady state, 1 p.u. of power (i.e., 1 GW) is transmitted from Network 1, through the AC cable and DC stations, to Network 2. The simplified network diagram shown in Figure 29, although it presents fewer components than Figure 27, includes all the parts described earlier and will be used for easier assignment of current and voltage values to specific points in the network. Points previously marked in Figure 27 (1, 2, and 3) correspond to the points shown in Figure 29.

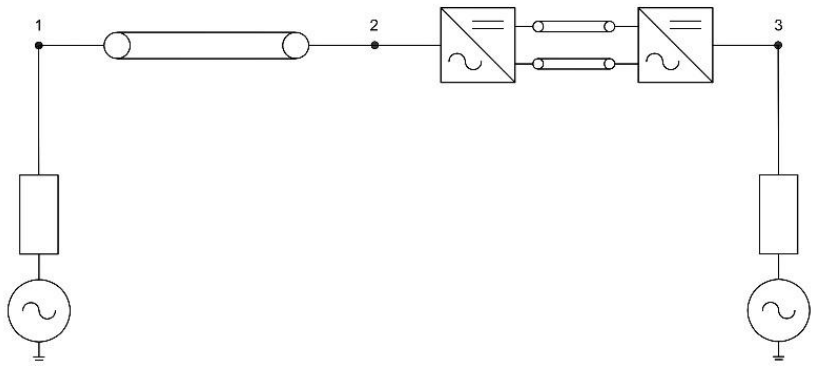

Figure 29. Simplified network topology

Upon initiating the simulation with the specified parameters, it was observed that currents and voltages quickly stabilized. However, the magnetic flux in Converter Transformer 1 could not stabilize, even though the simulation time was significantly extended. Although this process tends to stabilize, it is extremely slow. Therefore, additional resistance was introduced into the system to accelerate the process. Further investigation revealed that the cause of it was a small DC current component flowing through the windings, which induces a DC magnetic flux in the core. This phenomenon is characteristic for converter transformers and has been addressed in many studies as well as in IEC standards [20]. To resolve this issue and keep the simulation time at a reasonable and feasible level, a ground resistor R_{star} of 10 Ω was added to each phase of the AC side (star configuration) of the transformers. This is also one of the methods to address the DC bias problem in transformers as described in [21]. Although it causes additional losses in the actual system, it will be used in subsequent result presentations as it represents the simplest solution for achieving steady state within reasonable timeframes. The stabilization of flux with and without resistors is shown in Figure 30. This implementation allowed achieving steady state after 40 seconds of simulation, making further analyses time-consuming but still within reasonable limits. The implemented solution is therefore present in all further analyses.

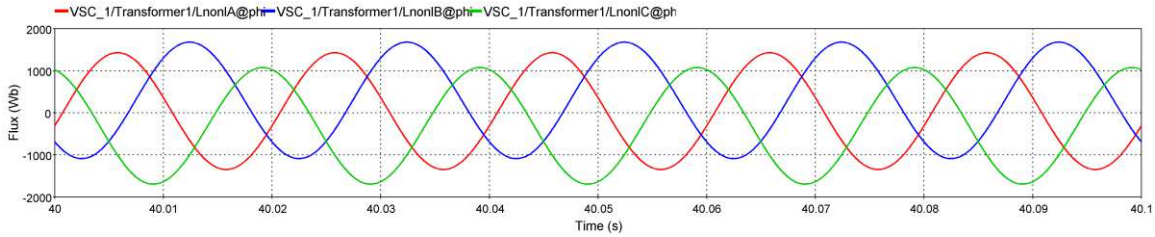

a) before implementation of $R_{star} = 10\ \Omega$

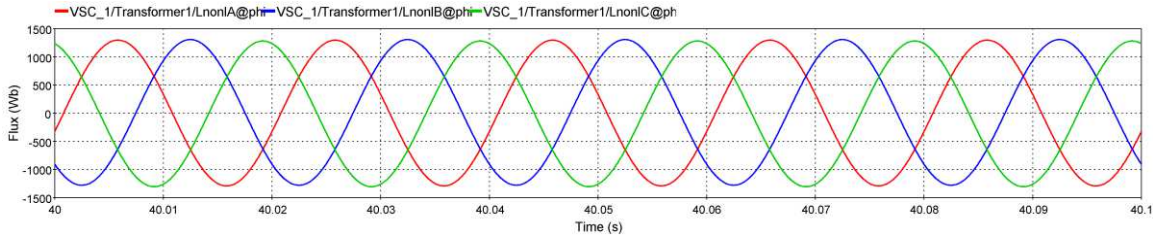

b) after implementation of $R_{star} = 10\ \Omega$

Figure 30. Magnetic flux in Converter Transformer 1 before and after implementation of resistance suppression

Once the steady state was achieved, the voltage and current values were checked to ensure the proper operation of the system. The AC RMS phase values of currents and voltages at each point, as shown in Figure 27 and Figure 29, are presented in Table 5. It is interesting to note that V_3 is higher than V_2, despite being further from the reference Equivalent network 1. The reason for this is the DC system, which helps stabilize the voltage. Without it, the voltage in a conventional AC system would continue to decrease, requiring the use of other methods to stabilize it. It was also observed that the current from the beginning of the network decreased from the initial 1.6 kA to 1.3 kA, which was caused by the losses in the converters as well as the parasitic capacitances of the cables.

Table 5. Steady state values of currents and voltages

RMS phase value	
current	voltage
$I_1 = 1.6\ kA$	$V_1 = 231\ kV$
$I_2 = 1.5\ kA$	$V_2 = 219\ kV$
$I_3 = 1.3\ kA$	$V_3 = 231\ kV$

The DC values of currents and voltages correspond to the specified ones for MMC stations: a pole-to-pole DC voltage of 640 kV, while the current in each pole is 1.5 kA.

After achieving steady state, frequency response analysis of the system can begin according to the methodology described in Subchapter 4.3, using time-domain simulations. The used procedure is detailed in the following Subchapter 7.1.

7.1. Frequency Response

The first step in resonance analysis is obtaining the frequency response of the network in order to gain an insight into the behaviour of the network at various frequencies, not only at the nominal one of 50 Hz. The used method involves obtaining the network's frequency response through numerical simulations in the time domain using the small signal perturbation method as described in [4] and [7]. The uniqueness of the frequency response of a system containing DC components, which are in this example MMC converters, lies in the fact that it cannot be performed in numerical programs in the conventional way, as is the case with completely AC systems (executed using generic blocks that observe the impedance between two selected points, with the process already taking place in the frequency domain). Instead, the system must first be in a steady state, so the transition from time domain to the frequency domain is a must. Therefore, in addition to using numerical tools for time-domain analyses, tools for data processing and computation, such as MATLAB, are also used for transitioning to the frequency domain. The transition from the time to the frequency domain was carried out following the methodology shown in Figure 8.

Following this methodology, frequency response is analysed using the diagram shown in Figure 31. Firstly, the network must achieve a steady state, which happens at the 40^{th} second. However, at the 45^{th} second, a small perturbation current is injected at the previously defined point of the network where the impedance is to be observed. Perturbation current is a sinusoidal current with an amplitude of 5 A, which is small enough to avoid significant changes in steady state but large enough to be noticeable. By injecting the perturbation, the steady state was not disturbed, but its harmonic composition was slightly changed around the injection frequency. Due to the possibility of the presence of harmonics in the network, which are not part of the perturbation, the harmonic spectrum was recorded before the perturbation. The frequency of the perturbation current is varied to obtain the desired system response. For example, to analyse the system at 100 Hz, a 100 Hz current is injected. In this

way, the time domain simulation encompasses both the network in steady state and the network disturbed by a small signal. During this process, current waveforms from each side of the injection point (towards Network 1 and towards Network 2), as well as the voltage waveforms at the injection point, are recorded. These recordings serve as a starting point for the transition from the time domain to the frequency domain. Although this method sounds complicated, it is based on the simple principle of a current divider.

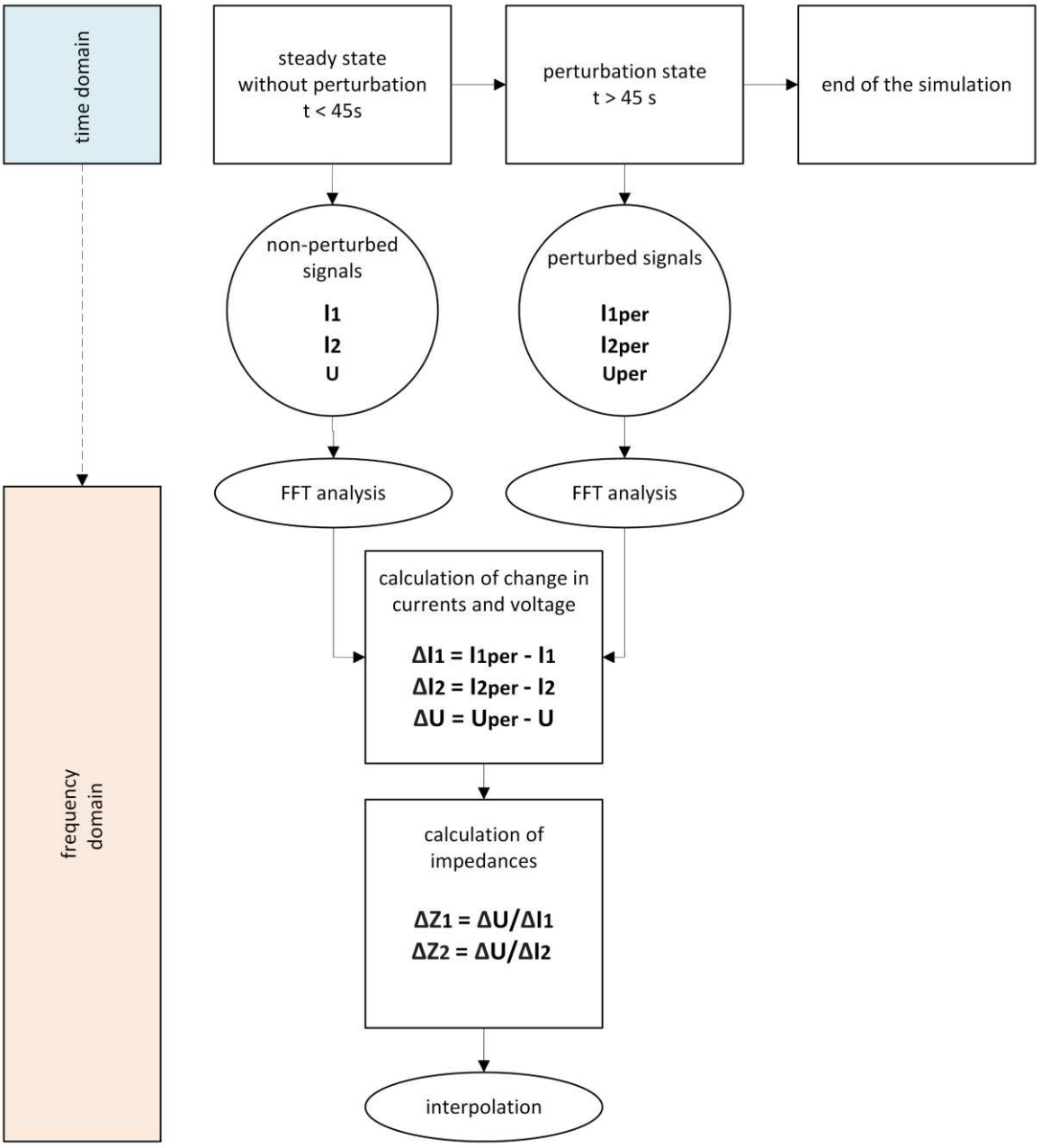

Figure 31. Process for obtaining the frequency response of the network

The perturbation method works by distributing the injected 5 A harmonic current into components I_{1per} and I_{2per} depending on the impedance that each side of the network

provide at the given frequency. Before the perturbation, the waveforms of I_1 and I_2 are equal as there is no perturbation, but there is a difference in their phase angles since the network is observed from the opposite polarity side. It is important to record currents and voltage signals at the injection point, both before and after the perturbation, because only in this way real changes due to the perturbation can be determined, which are then used to calculate the impedances for each side of the network. The way of functioning of the small signal perturbation method is shown in Figure 32, where the measured values are marked in blue, and the parametric value in red.

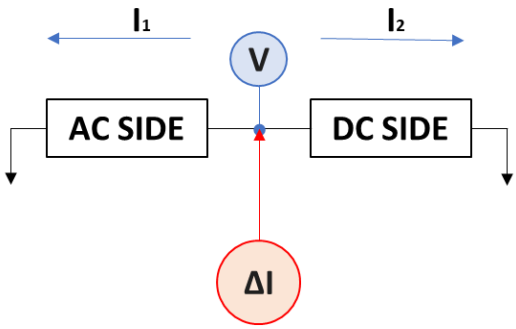

Figure 32. Distribution of perturbation in the network

After the time domain simulation, Fast Fourier Transformation (FFT) available in EMTP has been used, which enables the transition to the frequency domain. The analysis is performed on the currents and voltage waveforms before and after the perturbation. The amplitudes and phases of the currents and voltage for each injected frequency are recorded. In this way, using EMTP provides the necessary data, which are then further processed.

Time domain simulation is repeated for frequencies ranging from 1 Hz to 5000 Hz with various step sizes. Up to nominal 50 Hz frequency, the injected perturbation frequency does not have a constant step (1, 5, 10, 25, 35, 50 Hz perturbation was injected), after which a frequency step of 25 Hz is used until reaching 250 Hz. The reason for this is the behaviour of the converter, which changes its response in the frequency range around 100 Hz, as at higher frequencies it behaves like an inductor with increasing impedance magnitude. So, after that a 50 Hz frequency step is used, which was further increased to 250 Hz after reaching the 750 Hz.

Currents and voltage values before and after perturbation are recorded for each injected frequency using the FFT available in EMTP and then processed using MATLAB to calculate the impedances. The extracted harmonics are then subtracted to determine changes, and

these changes are used to calculate impedance at the perturbation point using Ohm's law. The resulting impedance points are then interpolated for streamlined analysis.

The described procedure was therefore applied to the steady state values when transmitting power of 1 p.u. where the perturbation current is injected at two different locations, at the Point 1 and Point 2, as shown in Figure 33. It is important to note that the frequency analysis was conducted using only phase A, and the presented results pertain to only one phase. However, this should not pose a problem because the network is symmetrical.

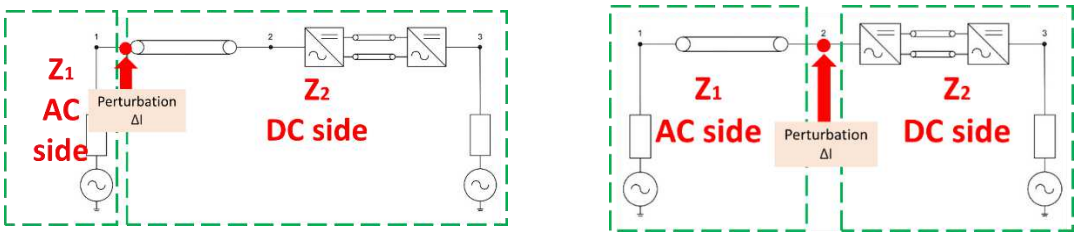

a) location 1 b) location 2

Figure 33. Network configuration for obtaining frequency response of the network

The representation of the obtained impedances at each perturbation point and the results derived from interpolation for both locations can be seen in Figure 34. The impedances Z_1 and Z_2 relate to two sides of the network, where Z_1 pertains to the AC side, while it only consists of the AC components, while Z_2 pertains to the DC side, including AC system but also two MMC stations and DC cable for both locations as is depicted in Figure 33.

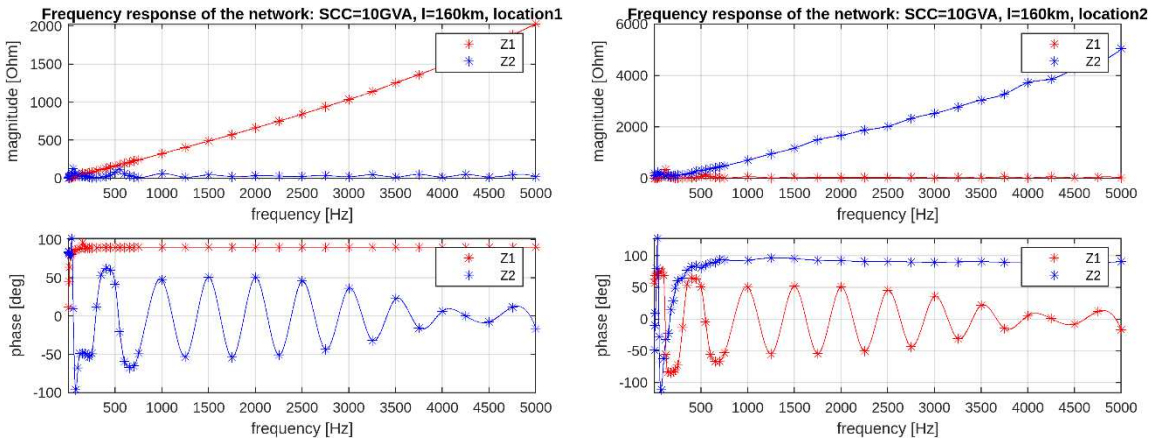

a) location 1 b) location 2

Figure 34. Frequency response of the network, base case – location 1 and location 2

For location 1, impedance Z_1 contains only the Equivalent network 1, while impedance Z_2 includes everything else, such as the AC cable, two MMC stations, the DC cable, and the

Equivalent network 2. Location 2 differs only in that the impedance of the AC cable is now included in impedance Z_1 and excluded from impedance Z_2, thus defining the case of interaction between the AC cable and the DC part of the network. In the following text, the term AC side will refer to impedance Z_1, and the term DC side will refer to impedance Z_2 despite the perturbation location to facilitate easier understanding.

After the frequency responses for both network locations were obtained, they were validated using a proven method to ensure that the small signal perturbation method was correctly applied. This validation was done by comparing the AC side frequency responses for both locations obtained through the frequency scan available in the EMTP. In this case, only the AC side could be verified using the generic function in EMTP due to the previously mentioned issue of bringing the converter to a steady state to ensure its correct operation. The results are shown in Figure 35. Frequency scan in EMTP was performed with a frequency step of 5 Hz, therefore the response at the very start is more accurate than obtained through small signal perturbation method in which various steps were used, but never as small as 5 Hz. The frequency steps used during the small signal perturbation method are described earlier in the text.

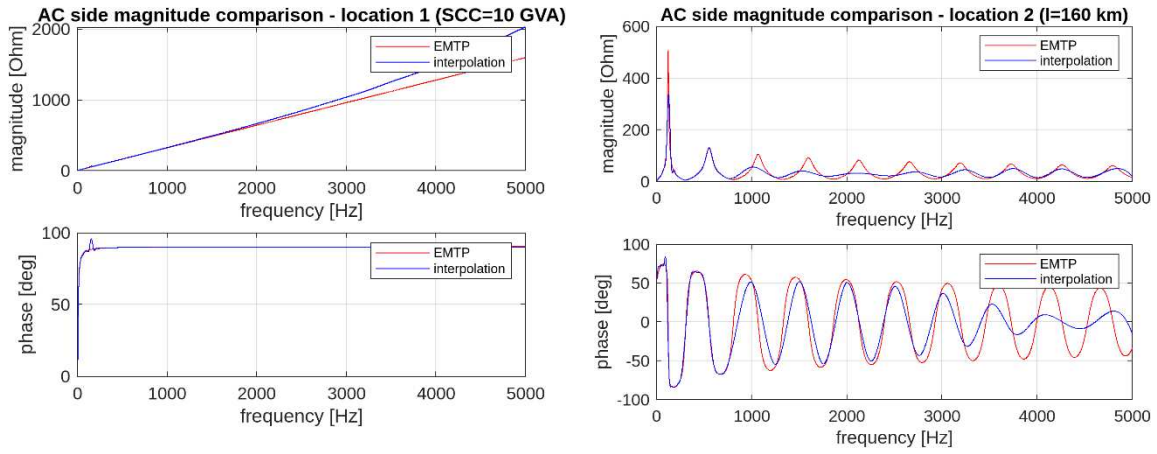

a) location 1 b) location 2

Figure 35. Validation of perturbation method using frequency scan in EMTP

Reviewing Figure 35, it was concluded that the obtained frequency response of the AC side impedance using the perturbation method closely matches the frequency response obtained with the frequency scan available in EMTP, especially at lower frequencies up to 750 Hz where the interval between injected frequencies is smaller so the process of interpolation is more accurate as more points were used. Although there are visible differences in frequencies higher than 750 Hz, especially in the magnitudes of the impedance, it is

important to note that these differences primarily arise from the interpolation introduced by the large frequency step, which was increased from 50 Hz to 250 Hz after injecting a perturbation current at 750 Hz.

When it comes to the frequency analysis for location 1, where the AC side contains only the Equivalent network 1 with a power of 10 GVA, a pure inductance is obtained, which increases with frequency, as expected, given that the Equivalent network 1 is described by a voltage source with an R-L load. This further opens up the possibility that more precise modelling of the equivalent network could impact its frequency response, considering that in this study it was described only using an R-L load, without additional capacitances.

On the other hand, for location 2, the AC side additionally includes an AC cable of 160 km in length, making it dominant compared to Equivalent network 1. The obtained response is typical for cable frequency analysis, where a series of resonant frequencies cause the cable to transition from inductive to capacitive mode and vice versa, reaching a peak magnitude at the transition point.

Nevertheless, for location 2 the frequency response obtained for the DC side is very similar to the previously shown response in Figure 24, and to [7] and [10] studies that have applied the same method, namely, the converters behave as inductors with very high impedance.

However, discrepancies are noticeable for both locations at higher frequencies, indicating the need to reduce the frequency step between the perturbation. Nevertheless, considering the Nyquist stability criterion, which states that resonance can only occur if the impedance magnitudes intersect, the significant differences in impedance magnitudes at higher frequencies led to focusing further analysis only on their frequency response up to 700 Hz. This approach ensures that used data and method are sufficiently accurate.

Based on everything, it can be concluded that the accuracy of the frequency responses is reduced, but still sufficient to determine the resonant frequency around which electrical resonance is possible.

Now that the method is considered correctly applied and the results are deemed sufficiently accurate, the Nyquist criterion can be easily applied to the frequency responses shown in Figure 34. By applying the Nyquist criterion, the system's resistance to potential resonance at stated operating point at both locations in the network are evaluated. For resonance to occur, impedance equality on both sides is required. Due to the significant difference in impedance magnitude shown earlier in Figure 34, Figure 36 is additionally presented, which

displays the same response but up to a frequency of 700 Hz instead of 5000 Hz. This approach also facilitates easier application of the Nyquist criterion.

The significant capacitance of the cable notably reduces the resonant frequency, causing the intersection of the magnitudes of individual impedance sides at much lower frequencies compared to overhead lines, as shown in [7]. This phenomenon directly suggests that the possibility of resonance is thus limited to much lower frequencies (around 100 Hz) primarily due to the large difference in impedance magnitudes at higher frequencies. However, for location 1, there is also a significant difference in impedance magnitude, with Network 1 representing a much larger impedance than the rest of the network defined as DC side impedance.

Before applying the Nyquist criterion, a rough rule of passivity can be used, which states that resonance will not occur if the phase angle of the impedances is kept within -90° to 90° limit. The non-passive behaviour of the DC side impedances becomes apparent for the location 2 in the range from 58 to 87 Hz, crossing -90°, which makes this frequency range particularly conducive to resonance (Z_2 brushed in red in Figure 36). If a network configuration that is purely inductive at which non-passive frequency range is connected to the observed DC side, resonance is guaranteed. At higher frequencies, the phase angle of the impedance Z_2 exceeds +90°. However, compared to the angle of Z_1, this does not pose a risk because the phase difference is far from being greater than 180°, ensuring compliance with the Nyquist criterion. Location 1 also exhibits this non-passive behaviour, but in a much narrower and higher frequency range (70-88 Hz), as the converter's non-passive impedance is further mitigated by the AC cable impedance observing from the Point 1.

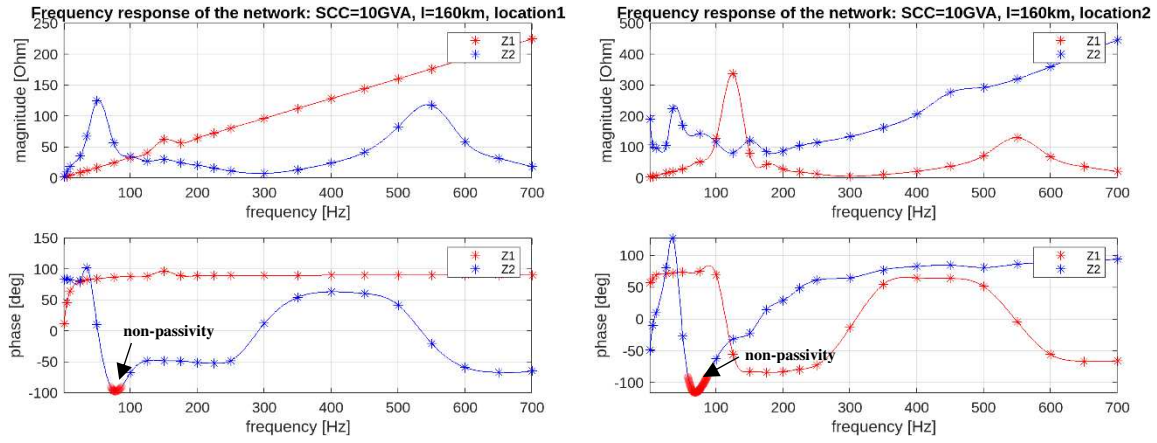

a) location 1 b) location 2

Figure 36. Frequency response of the network up to 700 Hz, base case – zoomed

By applying Nyquist criterion, magnitude responses are firstly examined after which the phase difference is observed. For the location 1, there is only one intersection point of the magnitude at around 90 Hz with a phase difference exceeding the 180° limit. Additionally, the non-passivity of the DC side was noted in the specified frequency and the AC side is inductive which goes in favour for the resonance as the DC side is capacitive. This all leads to the conclusion that the resonance at Point 1 for the base case, with the AC cable length of 160 km and SCC of the Network 1 of 10 GVA, is possible at around 90 Hz.

For the location 2, there are two intersection points of the impedance magnitude at around 100 and 150 Hz. However, unlike the previous case, the phase difference of the impedances did not exceed the 180° limit, indicating that resonance at Point 2 for the base case is not possible for the observed frequency spectrum. The reason for this is the passive behaviour of the DC side of the network at the intersection frequencies.

By observing the described baseline case, with 160 km AC cable length and SCC_1 of 10 GVA, it can also be noted that a long cable significantly reduces the value of the resonant frequency, posing a risk that it may reach the nominal 50 Hz, which is certainly not desirable. Additionally, it is interesting to note that for the same network topology and steady state, resonance is possible at Point 1, while it is not possible at Point 2, which highlights the complexity of resonance phenomena in its investigation.

From this, it can be concluded that at steady state Point 1 is more prone to resonance than Point 2, suggesting that the closer a point in the network is to the converter, does not necessarily mean it is more prone to resonance. The occurrence of resonance is not just a problem in HVDC systems; it has also appeared in traditional systems, but introducing the non-passivity behaviour of the DC parts further highlights the issue. The described situation applies only to the specific network configuration and the given steady state.

However, a significant issue with converters, and HVDC systems in general, is their non-passivity, specifically the negative real part of the impedance (i.e., negative resistance or negative damping). Figure 37 shows the real part of the impedance as a function of frequency for the baseline case for both locations, clearly illustrating the non-passivity of the DC side of the network since the damping D_2 achieves negative values. The non-passivity is also more pronounced at Point 2 than at Point 1, where the damping of the DC side, D_2, is more often negative than positive. It was also confirmed that the damping of the AC side D_1 is positive for both locations, which is expected since it does not contain a control system that is the main cause of the non-passivity of the DC side of the converter. In the literature [8],

the non-passive behaviour of type-IV turbine impedance is defined as one of the main causes of resonance, and active damping control has been proposed to avoid non-passive behaviour. The inexorable fact is that for 58% of the observed frequency range, the damping is negative for the DC side observed from Point 2, while observing from Point 1, it is negative for only 0.62% of the observed frequency range.

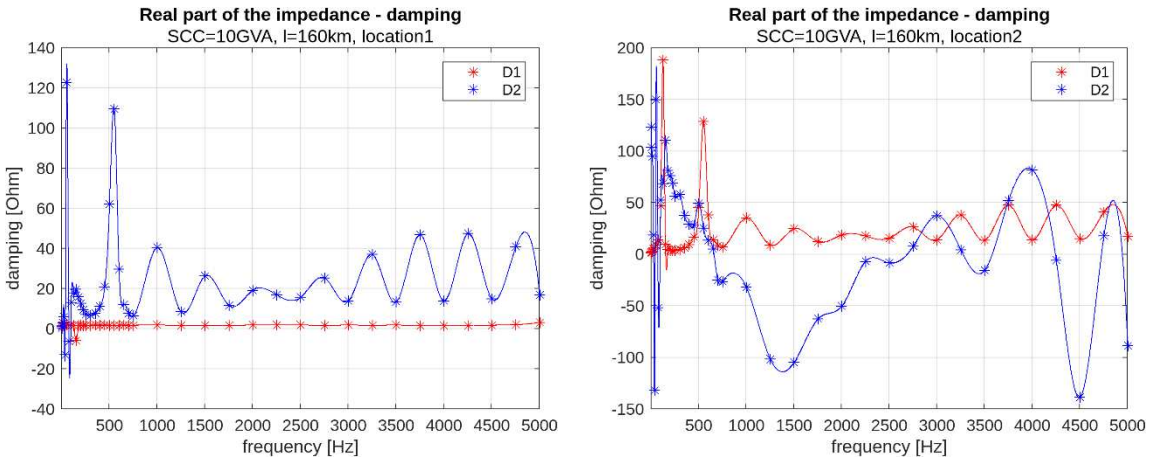

a) location 1

b) location 2

Figure 37. Real part of the impedances for both locations - base case

Based on the frequency response of the damping of the DC side for location 2, the following conclusion can be drawn. The DC side first exhibits non-passivity when operating in the capacitive mode (as shown in Figure 36), where resonance with an inductive network is possible at lower frequencies. However, in this case, this is not applicable since there are long AC cables, so the resonance is possible only for the location 1 where the AC side consists of pure inductance. Subsequently, the DC side achieves non-passivity when operating in the inductive mode at higher frequencies, allowing resonance with a capacitive network, i.e., with cables. However, the situation is not so straightforward, as at these higher frequencies, the significant difference in impedance magnitude between the AC and DC sides makes resonance practically impossible. These facts thus leave a narrow scope for inducing potential resonances between DC side and AC side for the given network topology. It can be said that this network topology and the obtained steady state successfully avoided the strongly emphasized non-passive area at Point 2.

Although the observed network is in a stable state at the nominal frequency of 50 Hz, the question remains as to what needs to be done to trigger the existing resonance at Point 1 and whether the overall network is sufficiently resilient to naturally dampen its occurrence. Common triggers for resonance include various faults or changes in network topology, even

lightning strikes. However, there are numerous factors that can initiate resonance, making it difficult to test every possible scenario. It is challenging to predict how the network will react to changes because each alteration also changes its frequency response. As a result, this type of analysis is time-consuming and requires consideration of many situations. Moreover, the significant difference in magnitude between the AC and DC sides further complicates the process.

Consequently, the same procedure for obtaining the frequency response was repeated for different lengths of the AC cable and for changes in the strength of Equivalent Network 1. Based on this, a sensitivity analysis was conducted by varying the length of the AC cable l and the strength SCC_1 of Equivalent Network 1 for both locations. The results are presented in the following Subchapter 7.1.1.

7.1.1. Sensitivity Analysis

The frequency responses of the network were analysed for different AC cable lengths (160 km, 80 km, and 40 km) as well as for changes in the strength of Network 1 (10 GVA and 4.7 GVA), and all with the aim of creating additional possibility for resonance, which in the base case is possible within a very narrow frequency range.

First, the influence of the strength of the Network 1 is analysed. If, in the baseline case with a 160 km long AC cable, the strength of Network 1 is changed from 10 GVA to 4.7 GVA, the possibility of resonance at Point 2 arises, as can be observed from the frequency response shown in Figure 38. This change suggests that if Network 1 is characterized as weak, resonances at steady state are possible both at Point 1 (at frequencies of 74-77 Hz) and at Point 2 (at frequencies of 75-76 Hz), while in the earlier case with the strong network, resonance was only possible at Point 1 (86-88 Hz). Also, the resonant frequency is slightly reduced.

Reducing the network strength change enabled resonance within the non-passivity range for both network locations, as reducing the power of Network 1 also increased the magnitude of the AC side impedance, allowing for the creation of impedance intersections at a lower frequency that corresponds to the non-passivity range.

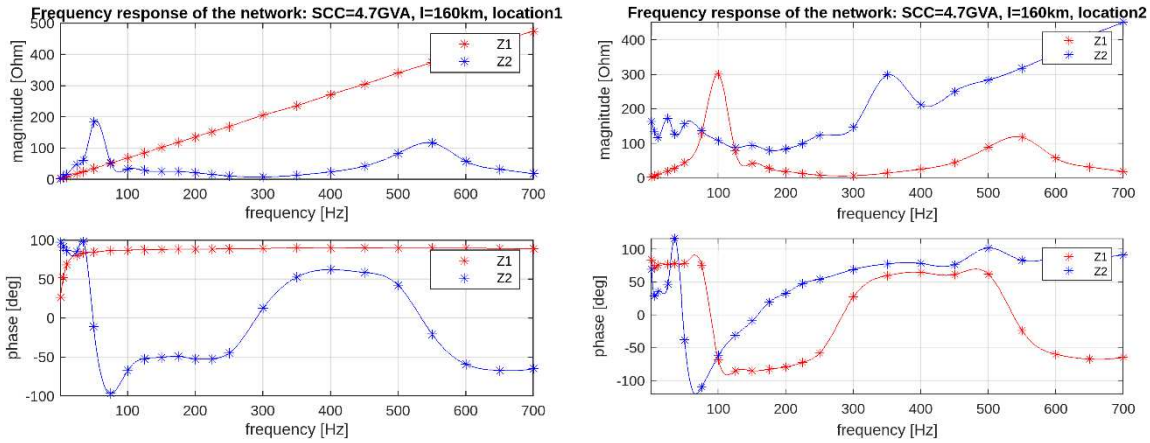

a) location 1

b) location 2

Figure 38. Frequency response of the network, l=160 km, SCC_l=4.7 GVA

The subsequent step was to examine how changing the length of the AC cable would affect the resonance conditions. Therefore, the length of the AC cable was reduced from 160 km to 80 km, while maintaining the existing strength of Network 1 at 10 GVA. The aim was to increase the magnitude of the AC side by decreasing the AC cable length to allow for more intersections with the magnitude of the DC side for location 2, which is one of the conditions of the Nyquist criterion. However, even with an AC cable length of 80 km, the impedance of the AC side remains significantly lower than that of the DC side. Therefore, the same approach was tried with a 40 km cable, but there were still no conditions for resonance, as shown in Figure 39, even though the AC side impedance becomes higher in magnitude. It was also observed that the intersection of impedances now occurs at higher frequencies, but the phase difference is still not large enough to satisfy the Nyquist criterion.

Based on the previous considerations, it can be concluded that with a strong network 1 (SCC_1 = 10 GVA), resonance is not possible, except in the case with a very long cable (l = 160 km), where resonance is only possible at Point 1, as shown in the baseline case depicted in Figure 34. This demonstrates that, given the network topology, changing the cable length has a minor effect on the possibility of resonance with a strong network. Therefore, a similar analysis was conducted with a weak network 1 (SCC_1 = 4.7 GVA), where resonance was observed at both points with a long AC cable of 160 km.

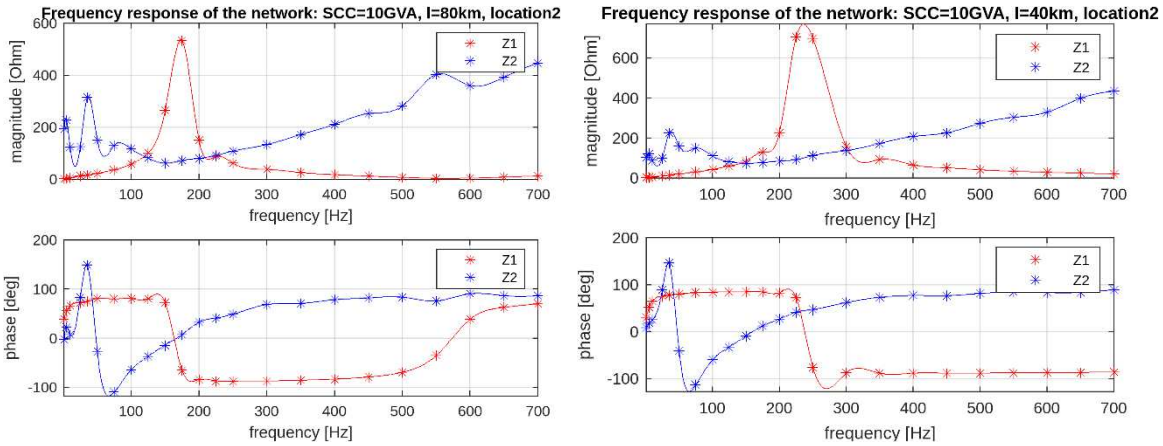

a) l=80 km b) l=40 km

Figure 39. The influence of the cable length on frequency response of the network - location 2

For a clearer overview of potential resonances, Table 6 can used. This table shows the possibility of resonance for the given network topology, depending on the cable length l and the strength of Network 1 SCC_1 for both locations. After applying the Nyquist criterion for the obtained frequency responses, the results of possible resonance are shown in Table 6, where an "X" indicates that resonance was not observed, and if resonance is possible, the corresponding frequency is listed.

It is important to note that the Nyquist criterion has been relaxed to account for the deviation in interpolation results of the frequency response of the network. Therefore, a difference in impedance magnitudes of 5 Ω and a phase difference of 170° were used as the conditions for satisfying the Nyquist criterion.

Table 6. Sensitivity analysis of possible resonance

	location 1	**location 2**
AC cable length	***l* = 160 km**	
***SCC*$_1$ = 10 GVA**	86 – 91 Hz	X
***SCC*$_1$ = 4.7 GVA**	75 – 76 Hz	76 Hz
AC cable length	***l* = 80 km**	
***SCC*$_1$ = 10 GVA**	X	X
***SCC*$_1$ = 4.7 GVA**	81-84 Hz	X
AC cable length	***l* = 40 km**	
***SCC*$_1$ = 10 GVA**	X	X
***SCC*$_1$ = 4.7 GVA**	X	X

From the data presented, it can be concluded that electrical resonance is favoured by weak networks and long cables. Under these conditions, resonance occurrences are more frequent compared to scenarios with strong networks and short cables. The reason for this is that by reducing the cable length, the resonant frequency shifts to higher values. However, the phase difference remains insufficient to satisfy the Nyquist criterion as the intersection points happen when the impedance is passive. However, it is important to note that these statements apply only to the examined network topology, so generalizing these findings should be done with caution.

The gained insights and the presented frequency responses have enhanced the understanding of the network's behaviour across the frequency spectrum from 1 Hz to 5000 Hz. They have also facilitated the induction of resonance in the time domain by altering the network's state. Examples of the network's behaviour during resonance for various scenarios are presented in the following Subchapter 7.2. In contrast to Subchapter 7.1, the focus will now be on analysing TOVs caused by triggered resonance in the time domain.

7.2. Time-domain Simulations

The frequency response of the network greatly aids in understanding its behaviour, but the goal of this work is to capture TOVs caused by resonance and to examine the overvoltages occurring in the network. During the study, two electrical resonant phenomena were successfully recorded: one caused by a temporary fault in the AC cable and the other by a change in the strength of Network 1.

A special case was also recorded in which electrical resonance and harmonic instability occur simultaneously, resulting from the interaction between the converter's protection system and the network. These cases are analysed separately in the following sections of this subchapter.

7.2.1. AC cable fault

Based on the frequency responses, it was concluded that a long AC cable of 160 km and a weak Equivalent Network 1 are most prone to resonance (Figure 38). Point 1 is susceptible to resonance at frequencies of 74-77 Hz, while Point 2 is susceptible at frequencies of 75-76 Hz. All other parameters are the same as in a base case.

Following this, time-domain simulations of single-phase and two-phase faults (including various phases of the cable) on the AC cable, specifically at Point 1, successfully triggered resonance. The most notable example of resonance is discussed in the following text. It involves a single-phase short circuit at Point 1 for phase A, specifically simulating a temporary fault at the 45^{th} second lasting 500 ms. Figure 40 depicts the location of an applied single-phase fault at Point 1. The goal was to shift the network from its nominal frequency of 50 Hz to the resonant point present at both Point 1 and Point 2, which was successfully achieved by considering the described fault.

It is interesting to note that when the magnetization branch of Converter Transformer 1 is excluded, no oscillation is observed. This underscores the importance of providing a detailed description of the system, as the potential for resonance could be overlooked if the magnetization branch is neglected.

During the fault, since no other protection system besides the one implemented in the MMC station was considered, the MMC blocks with a release delay of 20 ms because the voltage measured at the converter transformer dropped below 0.01 p.u.

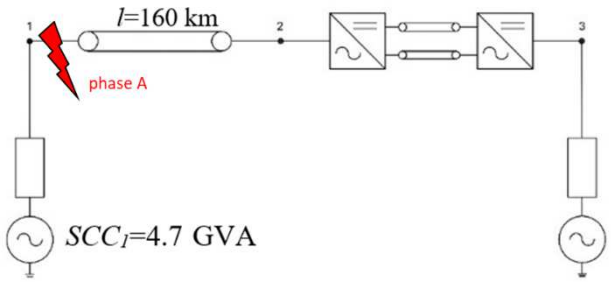

Figure 40. Location of a temporary fault that induces resonance; weak network and long AC cable

Figure 41 shows the time-domain voltage responses of each phase at Point 1 and Point 2 after clearing the fault, from which oscillations can be observed in all three phases at both locations (VLN refers to voltage-line-to-neutral). It is interesting to note that oscillations of the voltage at Point 3 are also observed, but they are not so expressed as they are easily damped.

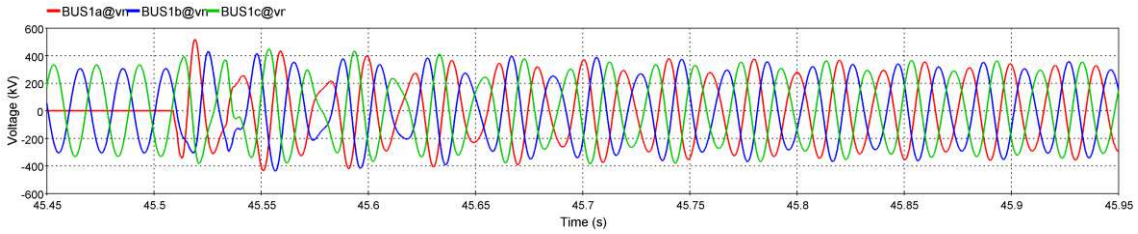

a) VLN voltage at Point 1

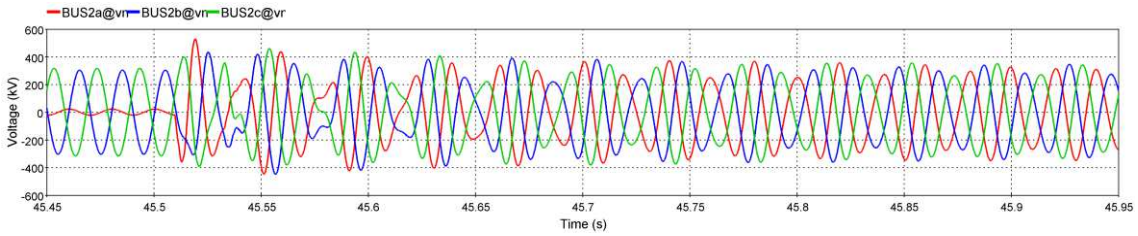

b) VLN voltage at Point 2

Figure 41. Oscillations of voltages at Point 1 and Point 2 after clearing of the fault

To determine that the observed oscillations are electrical resonance, an FFT analysis of the recorded voltage signals was conducted to confirm the presence of harmonics previously identified through the network's frequency responses as resonant. The analysis revealed the presence of a 76 Hz harmonic in all voltage signals (which is not present before the fault), though it is more pronounced at Point 2. This can be partially explained by the previously mentioned non-passivity of the DC side of the network. Figure 42 illustrates the damping

behaviour for the recorded frequency, showing that damping is negative for both locations, but more pronounced at location 2 for the resonant frequency.

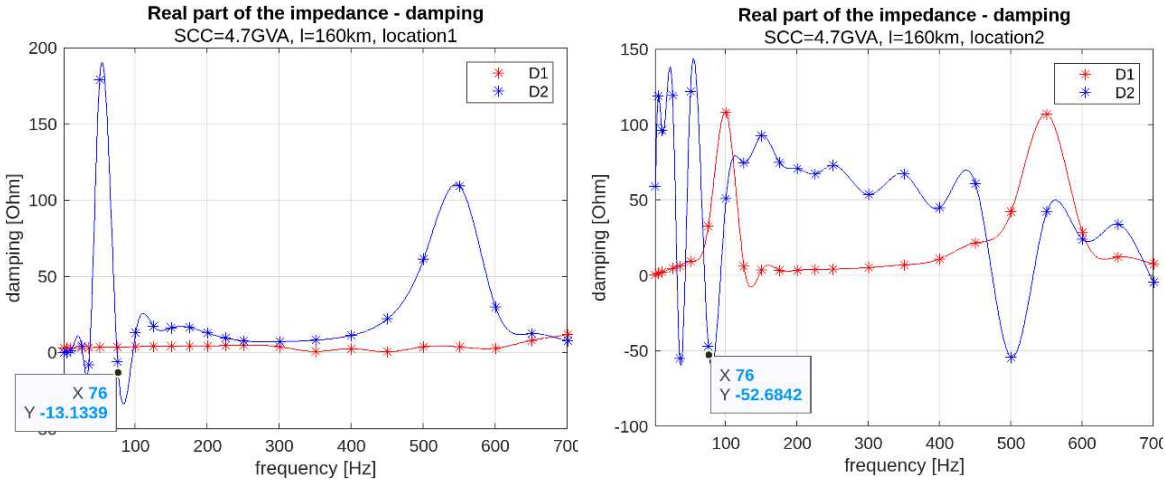

a) location 1 b) location 2

Figure 42. Frequency response of the damping for the recorded steady state

In addition to voltage oscillations, oscillations in magnetic flux and transformer core voltage at the side of the delta winding were also recorded (Figure 43). Moreover, the oscillation is also present in the DC part of the network, specifically affecting the active and reactive power of the converters as well as the DC current and voltage (Figure 44 and Figure 45). All this confirms that the whole system oscillates after a temporary failure.

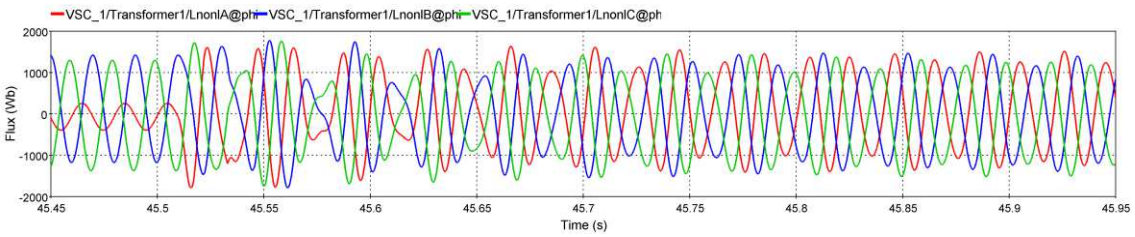

a) magnetic flux

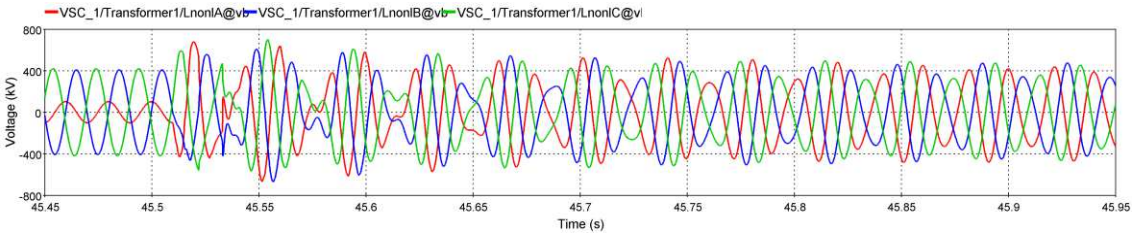

b) line-to-line voltage of the transformer core (delta configuration)

Figure 43. Oscillations in Converter Transformer 1

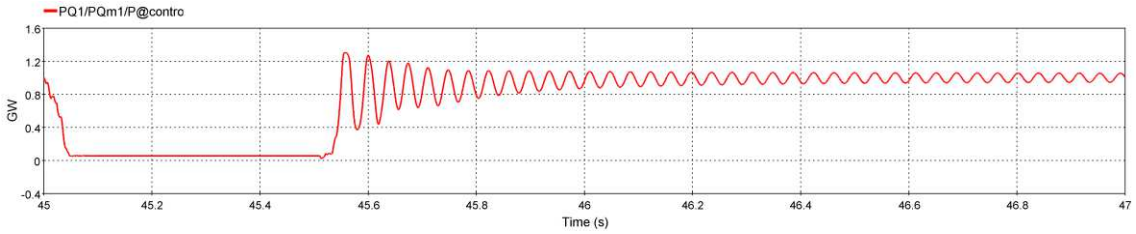

a) active power

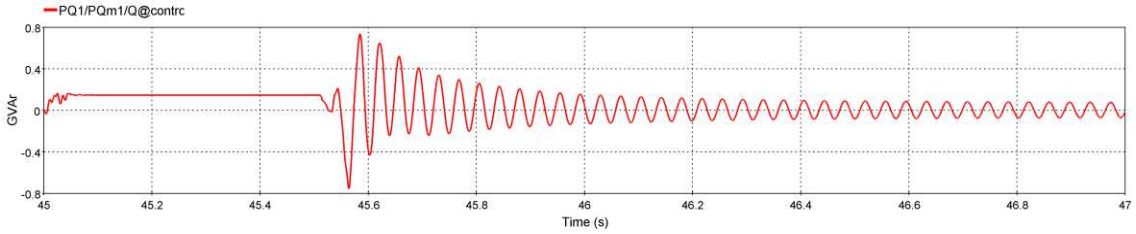

b) reactive power

Figure 44. Oscillations of active and reactive power in Converter 1

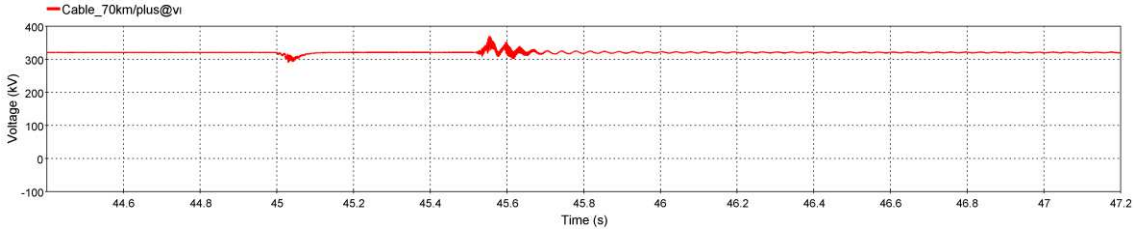

a) DC voltage (plus pole)

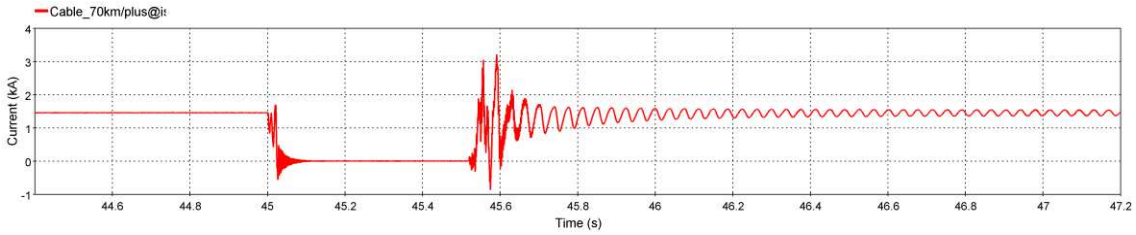

b) DC current (plus pole)

Figure 45. Oscillations of DC current and voltage

After observing the oscillations throughout the system caused by resonance, the behaviour of the 76 Hz induced voltage at Point 2, where the highest value was recorded, was also investigated. When observing the voltage waveform in phase A 1.5 seconds after the fault, focusing on the waveform over a one second duration (from 47th to 48th second), the induced 76 Hz harmonic constitutes 4.13% of the 50 Hz harmonic. It was also noted that the 50 Hz voltage component decreased slightly after the fault compared to its level before the fault,

by a very small amount, only around a hundred volts. The observed waveform of phase A, along with the FFT analysis results displaying the magnitudes of the fundamental 50 Hz and the induced 76 Hz harmonic, are shown in Figure 46.

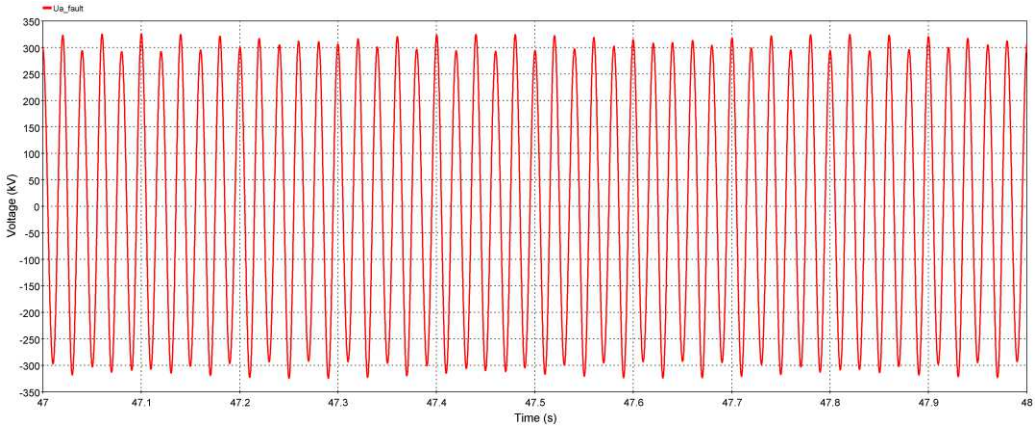

a) phase A voltage waveform for FFT analysis, $t \in [47,48]$ s

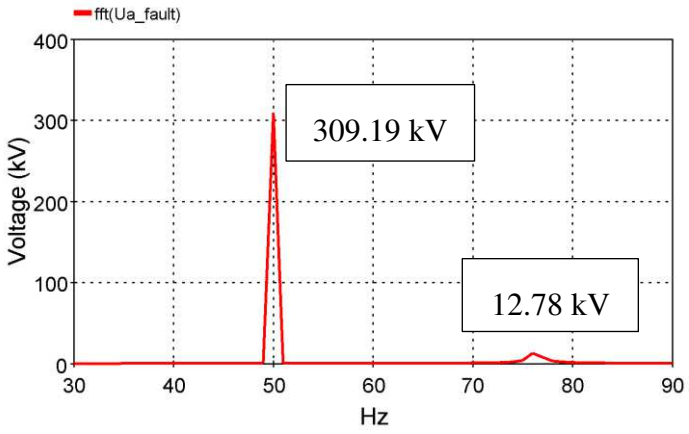

b) FFT results, 50 Hz and 76 Hz component

Figure 46. FFT analysis of voltage at Point 2, 1.5s after clearing of the fault

The induced 76 Hz component changes its magnitude as time passes after fault clearing, which is a characteristic of electrical resonance. Specifically, as voltage waveforms are observed over different time periods, the magnitude of the induced harmonic also varies. A graph shown in Figure 47 illustrates this phenomenon, from which it can be concluded that immediately after the fault, the 76 Hz harmonic is induced with a magnitude as high as 64 kV in phase A. However, its amplitude quickly diminishes to around 10 kV and then persists at this level for some time before it completely dissipates in the system. Although different time intervals were used for the FFT analysis, as shown in Figure 47, it can be concluded that the induced voltage initially exhibits a rather impressive magnitude, but its value rapidly decreases.

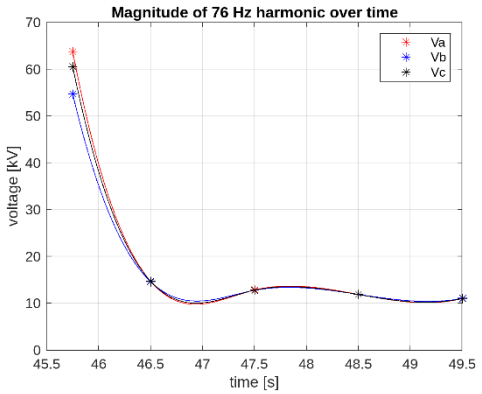

time limit for FFT analysis [s]	Va [kV]	Vb [kV]	Vc [kV]
45.5 – 46	63.645 > 20.55% of the 1st harmonic	54.62	60.43
46 – 47	14.62 > 4.72% of the 1st harmonic	14.55	14.63
47 – 48	12.78 > 4.13% of the 1st harmonic	12.72	12.74
48 – 49	11.85 > 3.83% of the 1st harmonic	11.85	11.81
49 – 50	10.95 > 3.55% of the 1st harmonic	10.99	10.97

a) magnitude of 76 Hz harmonic over time

b) data with observed time limits for FFT

Figure 47. Magnitude of 76 Hz harmonic after clearing of the fault

7.2.2. Changing the strength of the Network 1

The next recorded resonance phenomenon occurs when the power of Network 1 is changed from 10 GVA to 4.7 GVA. This change may be caused by disconnecting large generators or consumers or simply altering the network's topology. The goal is to transit the network from a stable state, where resonance is not possible for location 2, to a new state characterized by a weak network and a long cable (as in the base case with l = 160 km).

The frequency response of the AC side of the network for location 2 is shown in Figure 48, where it can be observed that by transitioning the network power from 10 GVA to 4.7 GVA (from the red curve to the black curve), resonance becomes possible for the range of 76-78 Hz which was stated earlier in the sensitivity analysis. The change in the frequency response of the DC side due to this alteration is very small, so the impedance response curve for the DC side is shown as the same for both cases.

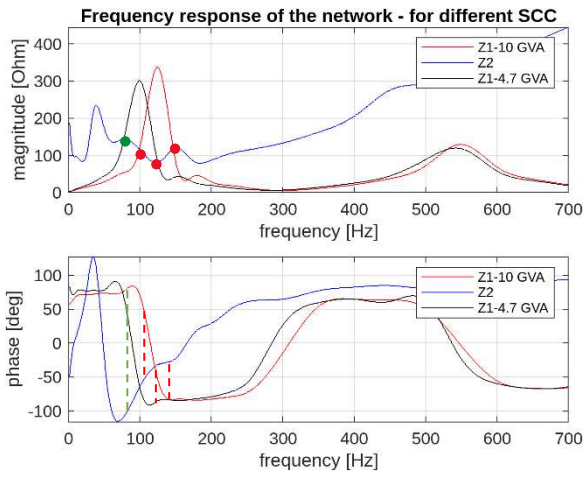

Figure 48. Change in frequency response due to the change of the Network 1 power

Following this, a time-domain simulation was conducted where the power of Network 1 was reduced from the existing 10 GVA to 4.7 GVA over a time span of 300 ms. The time-varying change of the SCC_1 parameter is defined as a stepped function as illustrated in Figure 49. The time response of the voltage at Point 2 during the observed occurrence is shown in Figure 50. The graph also highlights the boundaries of each change.

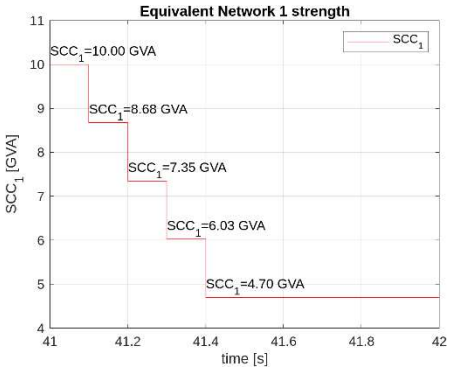

Figure 49. Time change of the Equivalent Network 1 strength

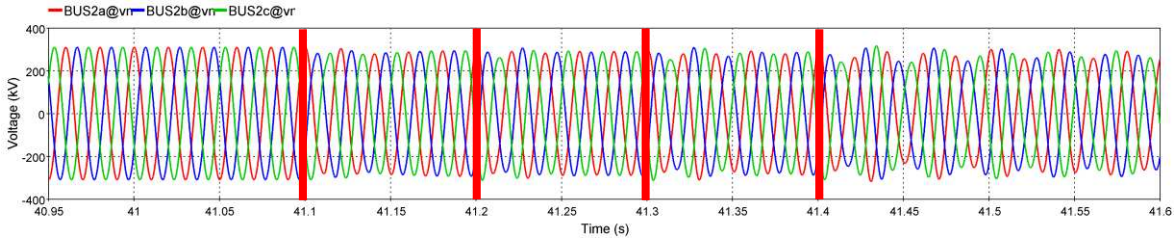

Figure 50. Voltage at Point 2 during change of the Equivalent Network 1 strength

It was also noted that there were significantly less fluctuations in active and reactive power in the converter then in previous case, as can be seen in Figure 51. The reason for this is the stepped change in power, which is not as abrupt as the previously observed fault. It is important to highlight that after this change, the converter's active power cannot be restored to the specified 1 p.u. for long, and instead, it remains at 0.9 p.u. as the described change has introduced a significant change in the operation of the system.

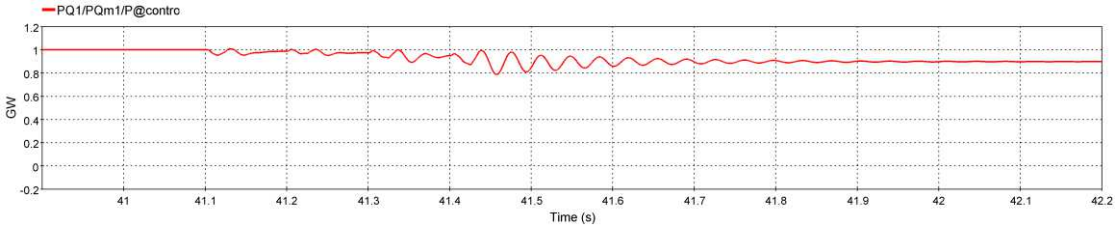

a) active power

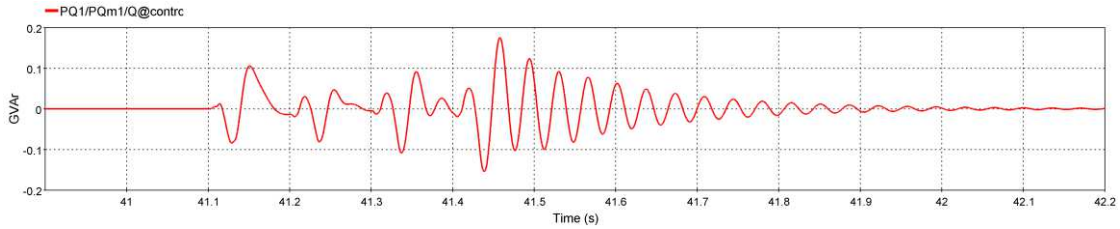

b) reactive power

Figure 51. Power response in Converter 1 after the stepped reduction of Network 1's strength

When the change is recorded, it is necessary to perform an FFT analysis of the observed voltage at Point 2 to confirm the electrical resonance. An FFT analysis of the voltage waveform at Point 2 is conducted after every change in the network's strength, but only after the last change resonant frequency was observed. The harmonic analysis confirmed the presence of a 78 Hz harmonic, identified through frequency analysis as resonant. Therefore, it can be said that the observed change in the network led to the induction of resonance.

The FFT analysis of the voltage waveform at Point 2 after the last network change for each phase is shown in Figure 52. Unlike the immediate 64 kV harmonic induced during the previous one-phase fault, the gradual change now led to an initial voltage induction of about 15 kV in each phase, which quickly diminishes. This fast magnitude decrease suggests that the system has sufficient damping to withstand the resonance, lasting only about 2 seconds. Furthermore, the resonance frequency shifted from 76 Hz to 78 Hz, primarily due to the DC side impedance response, which is slightly shifted to the right - a change not visually represented in Figure 38 due to its subtlety.

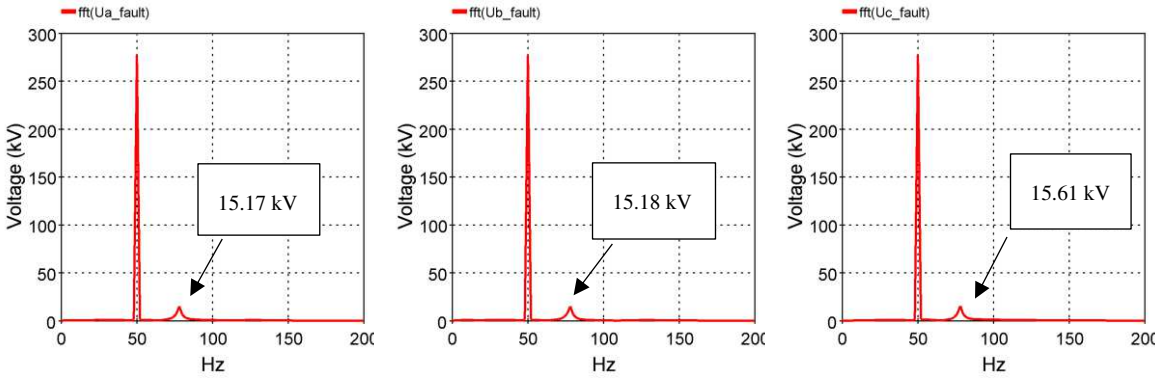

a) phase A b) phase B c) phase C

Figure 52. Comparison of 78 Hz and 50 Hz voltage magnitude at Point 2 after reducing the strength of the Network 1, $t \in [41.4, 41.9]$ s

To confirm the system's strong response to rapid changes, the same scenario was simulated as before by reducing the power of Network 1 from 10 GVA to 4.7 GVA. However, this time it was done rapidly as shown in Figure 53. Time response of a voltage at Point 2 with highlighted boundary of a rapid change is shown in Figure 54.

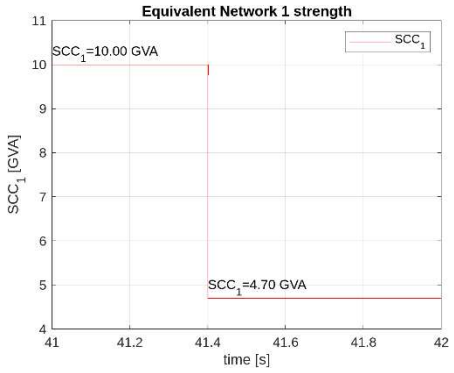

Figure 53. Time change of the Equivalent Network 1 strength – rapid case

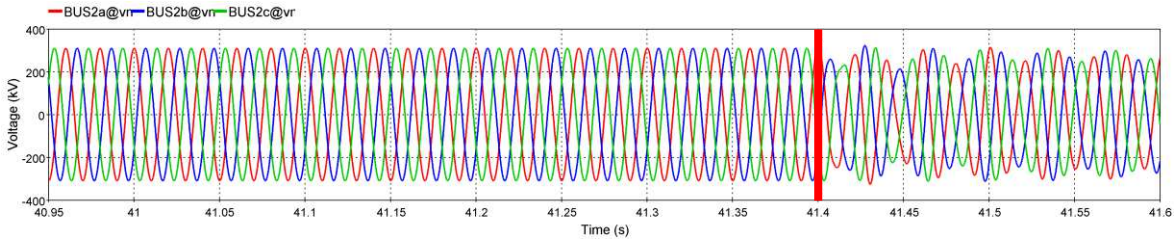

Figure 54. Voltage at Point 2 after rapid change of the Equivalent Network 1 strength

Oscillations of all previously mentioned values as in previously more stepped change were once again recorded. However, what particularly stood out was the increased oscillation magnitude of active and reactive power, with its response shown in Figure 55.

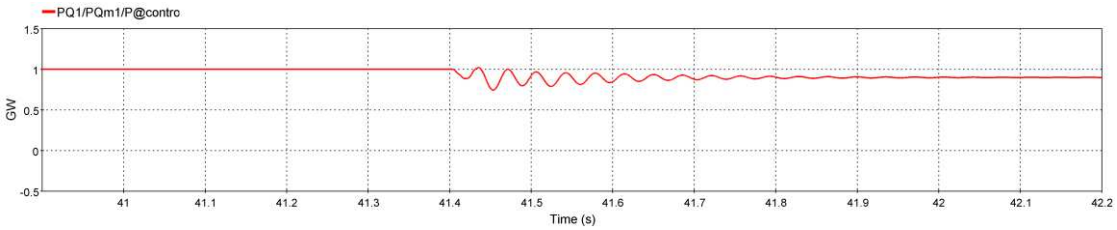

a) active power

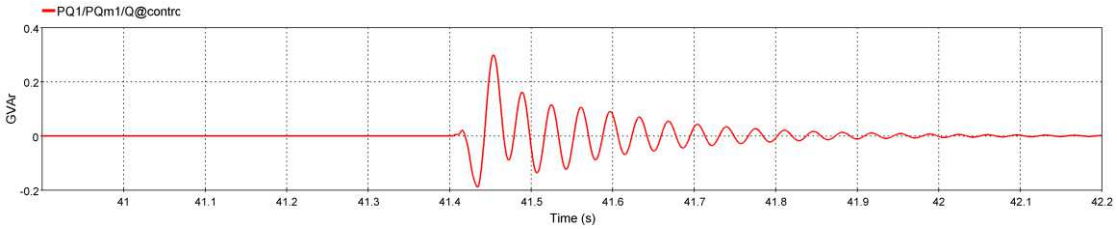

b) reactive power

Figure 55. Power response in Converter 1 after the rapid reduction of Network 1's strength

Comparing the recorded oscillations reveals that the system reacts more violently with a stepped change, as confirmed by the FFT analysis of the voltage at Point 2 shown in Figure 56. The magnitude of the 78 Hz harmonic due to a rapid change in power reaches approximately 20 kV, whereas, with a gradual change, it is about 15 kV. The previously mentioned study [16] shows that TOVs induction heavily depends on reactive power, which oscillates with higher magnitude during rapid changes, as evidenced by the comparison between Figure 55.b and Figure 51.b.

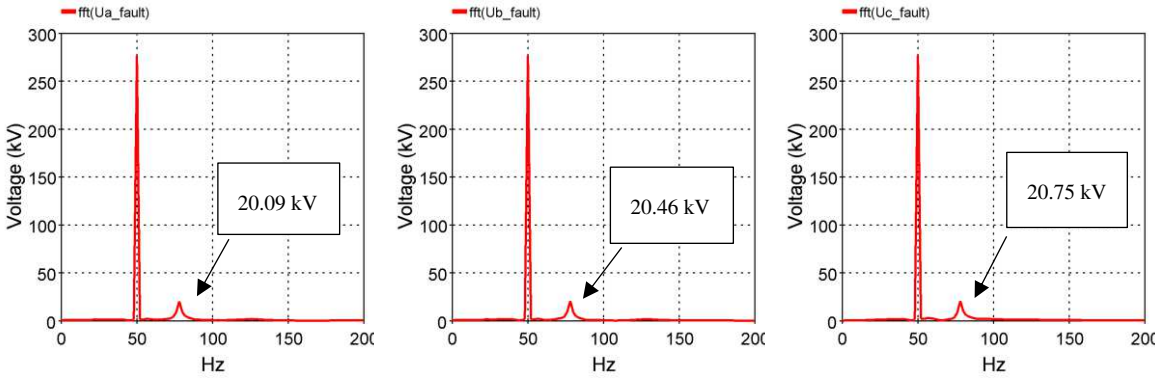

a) phase A b) phase B c) phase C

Figure 56. Comparison of 78 Hz and 50 Hz voltage magnitude at Point 2 after rapidly reducing the strength of the Network 1, $t \in [41.4, 41.9]$ s

7.2.3. Two Oscillation Problems at the Same Time

The two cases recorded so far pertain to network situations involving weak networks and long cables, where bringing the network to this unstable operating point has easily triggered electrical resonance. However, considering the behaviour of frequency responses based on the conducted sensitivity analysis, it is also possible to induce electrical resonance even in a network characterized as strong with short cables.

By simulating a single-phase fault at the 45th second, lasting for 500 ms, oscillations in the system were recorded. A graphical representation of the network, showing its main parameters, the strength of Network 1 of 10 GVA and the length of the AC cable of 10 km, and the fault location are provided in Figure 57. Recorded oscillation of the phase voltage at Point 2 is shown in Figure 58.

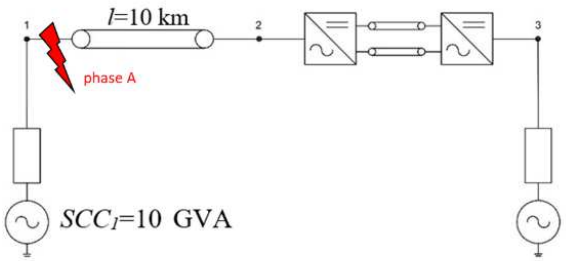

Figure 57. Location of a temporary fault that induces resonance; strong network and short AC cable

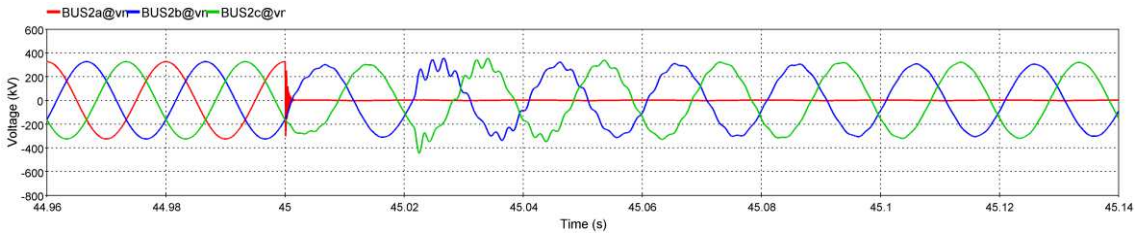

a) VLN voltage at Point 2 during the fault

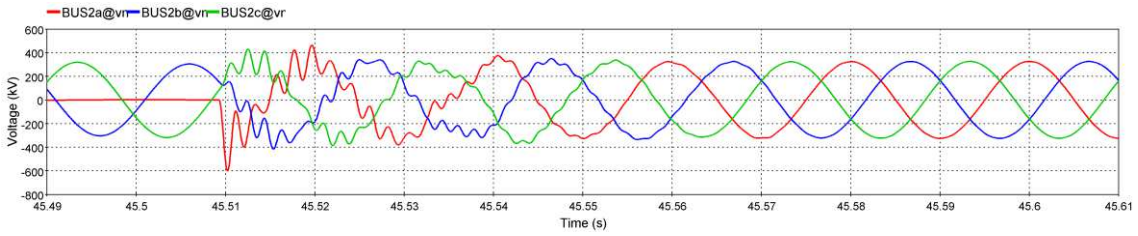

b) VLN voltage at Point 2 after clearing of the fault

Figure 58. Recorded oscillation of the voltage at Point 2

Based on the recorded oscillations in the system, a frequency analysis of the network was performed, with the results shown in Figure 59. According to the Nyquist criterion, electrical resonance was found to be possible in the frequency range around 600 Hz at both locations in the network, Point 1 and Point 2. Subsequently, an FFT analysis of the previously shown voltage was conducted to confirm the presence of a resonant frequency in the fundamental signal. The results of the FFT analysis for phase B, during and after the fault, are displayed in Figure 60.

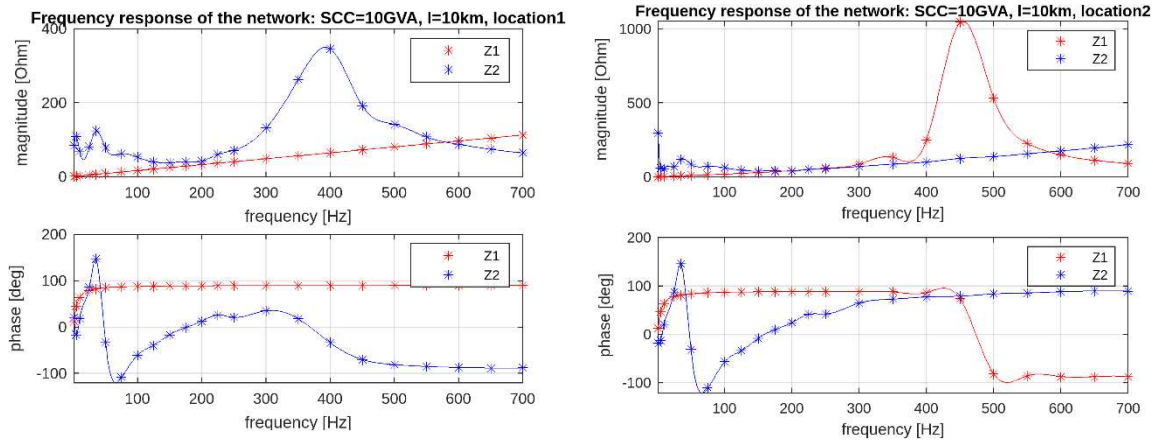

a) location 1 b) location 2

Figure 59. Frequency response of the network, l=10 km, SCC_1=10 GVA

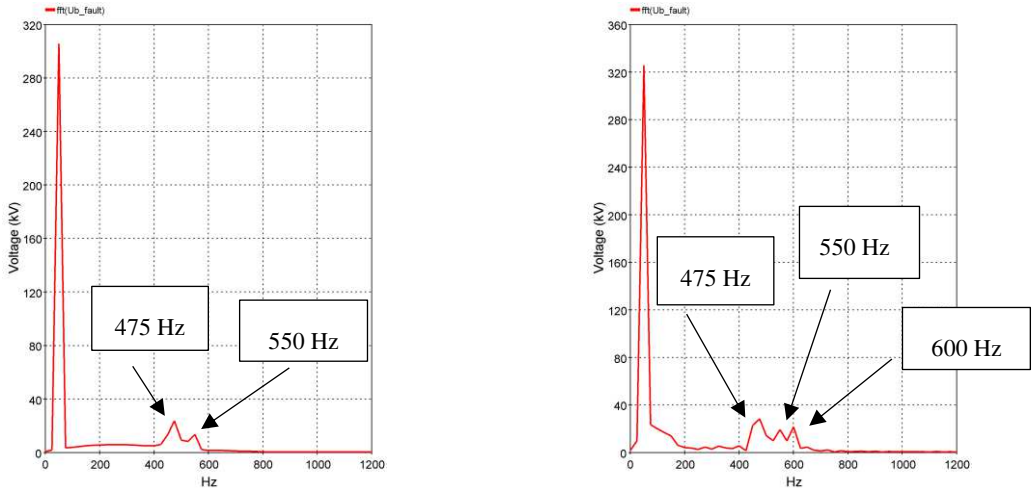

a) during the fault, $t \in [45.02, 45.06]$ s b) after the fault, $t \in [45.51, 45.55]$ s

Figure 60. FFT analysis of phase B voltage during and after one phase fault

FFT analysis revealed that, in addition to the presence of harmonics around 600 Hz, which, according to the Nyquist criterion, are identified as a result of electrical resonance, there are also other harmonics that cannot be explained by electrical resonance. To rule out the

possibility of interaction between the converter control system and the network, the simulation was repeated with the same parameters but with the protection system disabled. The protection system consists of a DC overcurrent and deep voltage sag detector, which is detailed in [19]. The same voltage responses at Point 2, as previously shown in Figure 58, are once again shown in Figure 61 but now excluding the protection system of the converter. Even from the recorded voltage waveforms during and after the fault, it can be observed that the waveform distortion is reduced or even disappeared during the fault, as confirmed by the FFT analysis of the voltage at Point 2 shown in Figure 62.

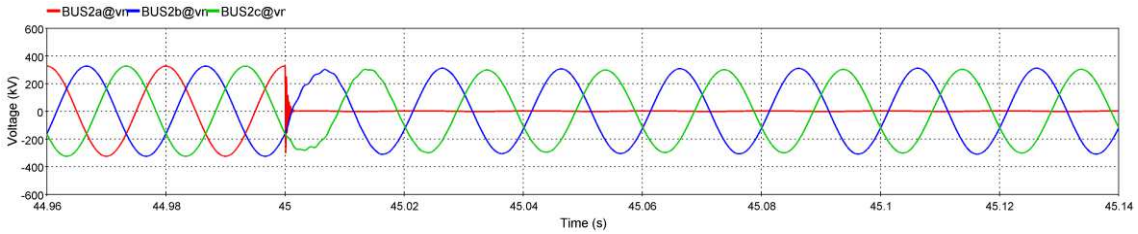

a) VLN voltage at Point 2 during the fault

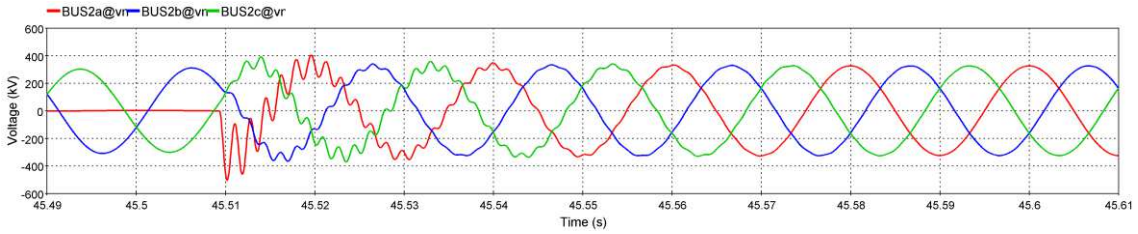

b) VLN voltage at Point 2 after clearing of the fault

Figure 61. Recorded oscillation of the voltage at Point 2 – converter protection system is excluded

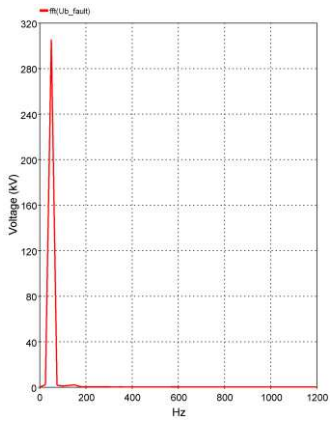

a) during the fault, $t \in [45.02, 45.06]$ s

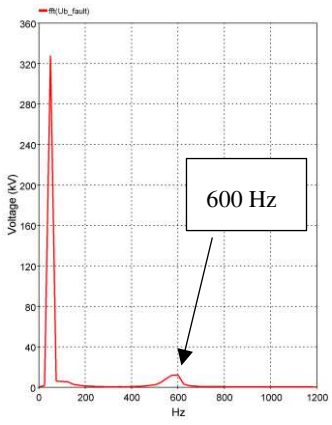

b) after the fault, $t \in [45.51, 45.55]$ s

Figure 62. FFT analysis of phase B voltage during and after one phase fault – excluding converter protection system

Based on the comparison of voltage waveforms and the results obtained from the FFT analysis, it can be concluded that the induction of 475 and 550 Hz harmonics was caused by interaction with the converter's protection system. This is confirmed by the fact that when the protection system was excluded, those additional harmonics were not induced, whereas, with the protection system included, this additional harmonic was present. In addition to the observed harmonic instability, 600 Hz electrical resonance was also recorded and confirmed based on the Nyquist criterion. A difference in the magnitude of the 600 Hz harmonics can also be observed with the protection system both enabled and disabled. Specifically, with the protection system enabled, the magnitude is 22 kV, whereas without the protection system, the magnitude is 12 kV. Thus, in addition to causing harmonic instability by inducing harmonics around 475 and 550 Hz, the protection system also contributed to the increase in the magnitude of the harmonics identified as a result of electrical resonance.

This case highlights that two types of oscillations can occur simultaneously, which makes an oscillation analysis very complex. This problem also underlines how the occurrence of oscillations is closely related to the converter parameters, which are often not well known. To further confirm the significant impact of the converter parameters on the system's operation, a single-phase fault was simulated once again with the protection system enabled, but now with a slower inner current control time constant.

In the base case, inner current control time constant was 0.01 s, and it has now been doubled to 0.02 s. Figure 63 shows the voltage time response at Point 2 after the fault with both faster and slower inner current control loops. The waveform indicates that the oscillations now have a longer duration, leading to the conclusion that a slower inner current control loop has a negative impact on the duration of the oscillations.

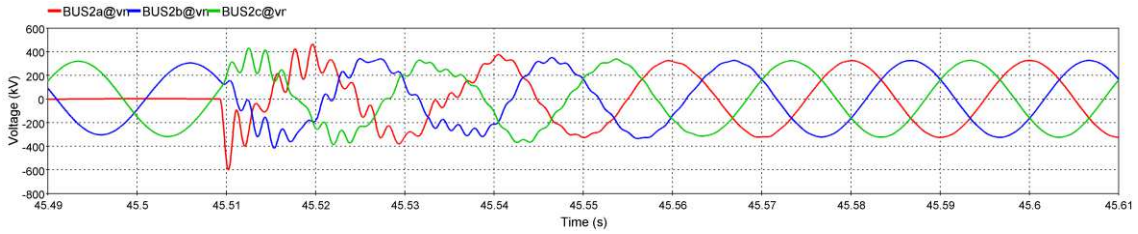

a) $T_{current}$ = 0.01 s

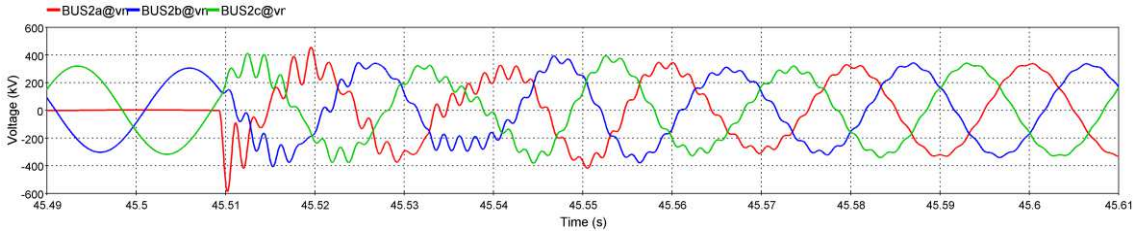

b) $T_{current}$ = 0.02 s

Figure 63. Recorded oscillation of the voltage at Point 2; with different inner current control loops

Recorded sensitivity of the system to such small but significant changes in converter parameters emphasizes the issue of modelling HVDC systems using black box models without knowing the true parameters of the converter due to the manufacturer's IP protection.

8. Ferroresonance

Another phenomenon explored in this paper is ferroresonance. Ferroresonance is a phenomenon whose term was introduced by Boucherot in 1920, although the first published work related to what was then called "transformer resonance" was by Bethenod in 1907. Today, the concept of ferroresonance is widely accepted and used in the industry [22]. There are a series of papers related to ferroresonance, but what connects all paper works related to it are electric circuits that have the following characteristics: a nonlinear saturable inductance (i.e., transformer), a capacitor, a voltage source, and low losses [22].

If the mentioned elements exist, there is a possibility of ferroresonance. It can be stated that ferroresonance represents a special case of electrical resonance where, instead of linear inductance, a nonlinear one is present, representing a transformer. Based on the network topology, there are also series and parallel ferroresonance [13]. However, in the context of transmission networks, series ferroresonance is commonly referred to, whereas parallel ferroresonance is more commonly associated with distribution networks featuring ungrounded or resonant neutral connections [13].

The problem of ferroresonance phenomena is mainly connected with potential transformers which start to oscillate with the breaker grading capacitance or compensated overhead lines. Those are well known cases which are usually mitigated by introducing additional losses in the system. Nevertheless, ferroresonance in the close vicinity of the HVDC stations has not been found to be widely reported in the literature [23].

The possibility of ferroresonance near converter stations introduces additional considerations their mitigation. As described in the literature [24], it is noted that converter controls can quickly suppress induced ferroresonance by incorporating additional damping into the system. This approach would help reduce the extra losses that arise from implementing long-term damping in the system.

Unfortunately, this study did not capture the case of ferroresonance due to the slow stabilization of the magnetic flux. Typically, a star point reactor prevents DC current from reaching the converter transformer, but since this parameter was not adjusted, resistors were used instead. The addition of a 10 Ω resistor in each phase inherently dampened the network, making ferroresonance difficult to induce.

Conclusion

Studying a mixed AC-DC networks presents a challenging and complex task, yet utilizing numerical tools like EMTP significantly eases this process by allowing simultaneous examination of control-loop interactions, system nonlinearity, as well as harmonic and resonant phenomena. The small signal perturbation method for obtaining the frequency response of a system that includes a converter is further complicated and time-consuming, especially when using interpolation and various frequency steps to accelerate the process, which can deviate from the real situation. However, obtaining the frequency response is possible and provides valuable insights into the network's behaviour at different frequencies.

Although the study began with the assumption that electrical resonance could occur between a capacitive network and an inductive converter, the situation is more complex. Despite the converter exhibiting inductive behaviour at higher frequencies and the network being capacitive, the significant difference in impedance magnitudes makes electrical resonance practically impossible according to the Nyquist criterion. Therefore, the resonant behaviour is confined to a narrow frequency range at somewhat lower frequencies where the network behaves inductively, the converter behaves capacitively, and additionally exhibits non-passive characteristics.

After successfully implementing the perturbation method and analysing the base case, a sensitivity analysis was conducted, as even small changes in network parameters can significantly affect its frequency response. Based on the sensitivity analysis, it has been determined that a network described as weak in configuration with long cables is more prone to resonance, particularly highlighting the non-passivity of the DC part of the network at frequencies identified as resonant.

Additionally, two pure electrical resonance phenomena in the time domain were simulated for weak networks and long cables. It was found that although TOVs of high values are initially induced, their magnitude rapidly drops to just a few kilovolts, suggesting that a network configured in this manner with the given parameters, while prone to resonance, can quickly dampen it.

A particularly interesting case was recorded in a strong network with a short cable in which two oscillations occurred simultaneously. One caused by electrical resonance, and the other by the interaction between the protection system and the network. It was also determined

that the protection system increased the resulting overvoltage, which additionally confirmed the sensitivity of the network's behaviour to small changes in the operation of the converter.

This work also attempted to explore ferroresonance. However, the challenge of asymmetry in the magnetic flux within the transformer core, caused by the presence of a DC component, hindered a systematic approach. Therefore, further research is necessary in this area. The proposal is to implement a star point reactor with a different value to avoid introducing additional damping into the system with the addition of resistors.

During the study of electrical resonance, an additional 10 Ω was added to each phase of the transformer, raising the question of how this resistance affected the system's frequency response, given that it also introduced additional damping. This study could also be improved by using more detailed converter models than Model 3, which was used in this study. This will further emphasize the nonlinearity of the whole system, which in this study only took the nonlinearity of the converter transformer near the AC cable. It is also possible to provide a better frequency description of equivalent networks, which in this case are represented only by a voltage source with an R-L load. Improvements are also possible in the implementation of other protective systems, besides the one implemented in the MMC stations.

Further research and enhancements of transformer and converter models can provide deeper insights into the behaviour of resonances in complex power systems. This opens opportunities to increase network stability, especially in the context of challenges such as ferroresonance.

Bibliography

[1] C. Buchhagen, C. Rauscher, A. Menze and J. Jung, “BorWin1 - First Experiences with Harmonics Interactions in Converter Dominated Grids,” in *International ETG Congress*, Bonn, 2015.

[2] O. C. Sacinci, “Modeling of the Modular Multilevel Converter using Dynamic Phasors, Reduced-Order Models for Small-Signal Stability Analysis,” 2022.

[3] JWG.C4/B4.52, “Guidelines for Subsynchronous Oscillation Studies in Power Electronics Dominated Power Systems,” CIGRE, 2023.

[4] WG.B4.67, “AC Side Harmonics and Appropriate Harmonic Limits for VSC HVDC,” CIGRE, 2019.

[5] WGC4.49, “Multi-frequency stability based of converter-based modern power systems,” CIGRE, 2024.

[6] Z. Yan, J. Xu, G. Yu, E. Bai and W. Chen, “Detailed Wideband Impedance Modeling and Resonance Analysis of Grid-Connected Modular Multilevel Converter,” *Energies,* 2023.

[7] H. Saad, Y. Fillion, Deschanvers, S. and Y. Vernay, “On Resonance and Harmonics in HVDC-MMC Station Connected to AC Grid,” *IEEE TRANSACTIONS ON POWER DELIVERY,* vol. 32, no. 3, pp. 1565-1573, 2017.

[8] J. Sun, I. Vieto and C. Buchhagen, “High-frequency Resonance in HVDC and Wind Systems: Root Causes and Solutions,” IET Renawable Power Generation, 2022.

[9] L. Harnefors, M. Bongiorno and S. Lundberg, “Input-Admittance Calculation and Shaping for Controlled Voltage-Source Converters,” *IEEE Transactions on Industrial Electronics,* vol. 54, no. 6, pp. 3323-3334, 2007.

[10] H. Saad, A. Schwob and Y. Vernay, “Study of Resonance Issues between HVDC link and Power System Components using EMT Simulations,” IEEE, 2018.

[11] L. Harnefors, X. Wang, A. G. Yepes and F. Blaabjerg, “Passivity-based Stability Assessment of Grid Connected VSC - an Overview,” *IEEE J. Emerg. Sel. Topics Power Electron,* vol. 4, no. 1, pp. 116-125, 2016.

[12] V. Milardić and B. Filipović-Grčić, “FER_Prenaponska zaštita,” 2024. [Online]. Available: https://www.fer.unizg.hr/predmet/prezas/materijali. [Accessed June 2024].

[13] WG.C4.307, “Resonance and Ferroresonance in Power Networks,” CIGRE, 2014.

[14] CIGRE and W. B4.71, “Application Guide for the Insulation Coordination of VSC-HVDC Stations,” CIGRE, 2017.

[15] G. Li, Y. Li and S. Xu, “A New High Frequency resonance Suppression Strategy for VSC-HVDC System,” CIGRE, 2022.

[16] H. Saad, “Study on TOV after Fault Recovery in VSC based HVDC Systems,” *IEEE Milan PowerTech,* 2019.

[17] “IEC TR 60071-4:2004; Insulation co-ordination – Part 4: Computational guide to insulation co-ordination and modelling of electrical networks,” IEC, 2004.

[18] CIGRE and WGB4.57, “Guide for the Development of Models for HVDC Converters in a HVDC Grid,” 2014.

[19] H. Saad, J. Mahseredjian and S. Dennetiere, “VSC-MMC STATION MODELS; Modular Multilevel Converter in EMTP-RV (Help Guide),” EMTP-RV, 2014.

[20] “IEC TS 60076-23:2018; Power transformers - Part 23: DC magnetic bias suppression device,” [Online]. Available: https://webstore.iec.ch/en/publication/31897. [Accessed July 2024].

[21] G. Zhao, G. Qiao, Z. Yu, T. Chen and Y. Wang, “A Review of Research on Transformer DC Bias Caused by HVDC Transmission,” in *Journal of Physics: Conference Seriec 2310*, 2022.

[22] D. Jacobson, “Examples of Ferroresonance in a High Voltage Power System,” IEEE, Manitoba.

[23] J. Rao, G. Bansal, T. Tulkiewicz and M. Ohrstrom, “Mitigation of Ferroresonance in Line Commutated HVDC Converter Interconnected with Series Compensated Overhead Line Transmission System,” IEEE EPEC, 2016.

[24] D. A. Woodford, “Solving the Ferroresonance Problem when Compensating a DC Converter Station with a Series Capacitor,” *IEEE,* vol. 11, no. 3, 1996.

[25] L. Harnefors, X. Wang, A. G. Yepes and F. Blaabjerg, “Passivity-Based Stability Assessment of Grid-Connected VSCs - An Overview,” IEEE, 2016.

[26] K. Ji, W. Chen, X. Wu and H. Pang, “High Frequency Stability Constraints Based MMC Controller Design Using NSGA-III Algorithm,” *CSEE JOURNAL OF POWER AND ENERGY SYSTEMS,* vol. 9, no. 2, pp. 623-633, 2023.

[27] C. B. Tambwe and R. Carpanen Pillay, “Investigating the Impact of HVDC on the Damping Subsynchronous Resonance,” in *International SAUPEC/RobMech/PRASA Conference*, 2020.

[28] J. Sun, “Impedance-based Stability Criterion for Grid Connected Inverters,” *IEEE TRANSACTIONS ON POWER ELECTRONICS,* vol. 26, no. 11, pp. 3075-3078, 2011.

Summary

RISK OF ELECTRIC RESONANCE OR FERRORESONANCE IN HVDC NETWORKS

HVDC networks, while offering a range of well-known advantages, also introduce an increased risk of oscillations. This study contributes to the investigation of electrical resonant phenomena associated with HVDC stations using numerical EMT simulations. However, ferroresonance phenomena were not addressed due to the challenges in stabilizing the transformer's magnetic flux caused by the DC component. The study concludes that electrical resonance is primarily pronounced in weak networks with long cables, as confirmed by applying Nyquist criterion on frequency responses. Two real cases were successfully simulated in the time domain by introducing network changes (transient fault and power strength changes) to activate the identified resonances. However, despite the greater risk of resonances in weak networks with long cables, the special case in a strong network with short cables was successfully simulated, where electrical resonance occurred at the same time, but also the interaction of the network with the protection system of the converter. The analysis of voltage waveforms led to the conclusion that the amplitude of the induced harmonic, resulting from oscillations, dissipates quickly because the network, as configured, has sufficient damping. In addition to the investigation of electrical resonance, the sensitivity of the network's response to changes in the parameters of the converter modeled as a black box was further confirmed.

Key words: electrical resonance, ferroresonance, HVDC networks

Sažetak

RIZIK OD POJAVE REZONANCIJE ILI FEROREZONANCIJE U VISOKONAPONSKIM MREŽAMA ISTOSMJERNOG NAPONA

HVDC mreže iako sa sobom donose niz sada već dobro znanih prednosti, ujedno unose u sustav povećani rizik od oscilacija. Ovim radom napravljen je doprinos u pogledu istraživanja električnih rezonantnih pojava povezanih s HVDC stanicama u numeričkom EMT programu, dok pojave ferorezonancije zbog problematike stabilizacije magnetskog toka jezgre transformatora zbog prisutstva DC komponente nisu razmotrene. Zaključeno je kako je električna rezonancija prije svega izražena u slabim mrežama s dugim kabelima. Navedeno je potvrđeno frekvencijskim odzivima mreže primjenjujući Nyquistov kriterij stabilnosti, a kasnije su uspješno simulirana dva slučaja rezonancije u vremenskoj domeni uvođenjem promjene stanja u mreži (prijelazni kvar te promjena snage mreže) kako bi se identificirana rezonancija aktivirala. Međutim, unatoč većem riziku od rezonancije u slabim mrežama s dugim kabelima, uspješno je simuliran i poseban slučaj u snažnoj mreži s kratkim kabelima, gdje je električna rezonancija nastupila istovremeno s interakcijom mreže sa zaštitnim sustavom pretvarača. Analizom valnih oblika napona zaključeno je kako se amplituda induciranog harmonika, nastalog kao posljedica rezonancije, vrlo brzo disipira u sustavu jer ovako konfigurirana mreža ima dovoljno prigušenja. Uz istraživanje električne rezonancije, dodatno je potvrđena osjetljivost reakcije mreže na promjene parametara pretvarača modeliranog kao crna kutija.

Ključne riječi: električna rezonancija, ferorezonancija, HVDC mreže

Abbreviations

APC	*Active Power Control*
AVC	*Alternating Voltage Control*
CBA	*Capacitor Balancing Algorithm*
CBA	*Capacitor Balancing Control*
CCC	*Circulating Current Control*
CCSC	*Circulating Current Suppression Control*
CI-D	*Control Interactions between a Devices*
CIGRE	*International Council on Large Electric Systems*
CI-N	*Control Interactions between a Device and the Network*
DFIG	*Doubly-Fed Induction Generator*
DVC	*Direct Voltage Control*
EMT	*Electromagnetic Transient*
EMTP	*Electromagnetic Transient Program*
FACTS	*Flexible AC Transmission System*
FFT	*Fast Fourier Transformation*
HVAC	*High Voltage Alternating Current*
HVDC	*High Voltage Direct Current*
IEC	*International Electrotechnical Commission*
IGE	*Induction Generator Effect*
IP	*Intellectual Property*
LCC	*Line Commutated Converter*
LL	*line-to-line*
MMC	*Modular Multilevel Converter*
OCC	*Output Current Control*

PCC	*Point of Common Connection*
PE	*Power Electronic*
PEDI	*Power Electronic Device Interactions*
PLL	*Phase-locked Loop*
RMS	*Root-mean-square*
RPC	*Reactive Power Control*
SCC	*Short Circuit Current*
SM	*Submodule*
SSCI	*Subsynchronous Controller Interactions*
SSR	*Subsynchronous Resonance*
SVC	*Static Var Compensator*
TB	*Technical Brochure*
TI-D	*Torsional Interaction against Devices*
TI-N	*Torsional Interaction against Network*
TOV	*Temporary Overvoltages*
VLN	*voltage-line-to-neutral*
VSC	*Voltage Source Converter*
WPP	*Wind Power Plant*